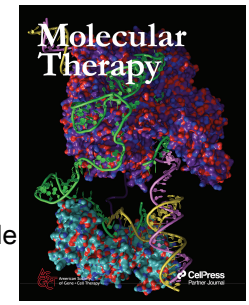

AAV-Mediated Exon Skipping Therapy for Usher Syndrome, Type 2A.

Stephanie A. Mauriac, Jiyoon Lee, Jingyuan Zhang, Jiahe Jin, Carl Nist-Lund, Camille T. Martin, Cristobal R. Von Muhlenbrock, Sydney O'Malley, Mary G. Chaves, Margot A. Madison, Kate Foster, Shinong Long, Chris Jacobs, Sripriya Ravindra Kumar, Silvia Ramirez, Justin Ichida, Karl R. Koehler, Jeffrey R. Holt, Gwenaëlle S.G. Géléoc

PII: S1525-0016(25)00767-1

DOI: https://doi.org/10.1016/j.ymthe.2025.09.038

Reference: YMTHE 7154

To appear in: *Molecular Therapy*

Received Date: 6 January 2025

Accepted Date: 19 September 2025

Please cite this article as: Mauriac SA, Lee J, Zhang J, Jin J, Nist-Lund C, Martin CT, Von Muhlenbrock CR, O'Malley S, Chaves MG, Madison MA, Foster K, Long S, Jacobs C, Kumar SR, Ramirez S, Ichida J, Koehler KR, Holt JR, Géléoc GSG, AAV-Mediated Exon Skipping Therapy for Usher Syndrome, Type 2A., *Molecular Therapy* (2025), doi: https://doi.org/10.1016/j.ymthe.2025.09.038.

AAV-Mediated Exon Skipping Therapy for Usher Syndrome, Type 2A.

Stephanie A. Mauriac[1], Jiyoon Lee[1*], Jingyuan Zhang[1*], Jiahe Jin[1], Carl Nist-Lund[1], Camille T. Martin[1], Cristobal R. Von Muhlenbrock[1], Sydney O'Malley[1], Mary G. Chaves[1], Margot A. Madison[1], Kate Foster[1], Shinong Long[2], Chris Jacobs[2], Sripriya Ravindra Kumar[2], Silvia Ramirez[2], Justin Ichida[2], Karl R. Koehler[1], Jeffrey R. Holt[1], Gwenaëlle S.G. Géléoc[1]

Department of Otolaryngology, Boston Children's Hospital and Harvard Medical School, Boston, MA, 02115, USA; BioMarin Pharmaceutical Inc., Novato, CA, USA

Corresponding Authors: jeffrey.holt@childrens.harvard.edu, gwenaelle.geleoc@childrens.harvard.edu karl.koehler@childrens.harvard.edu *equal contribution

ABSTRACT

Usher syndrome can cause loss of vision, hearing and balance. There are four clinical subtypes, USH1 through 4, which are associated with mutations in genes important for structure, function and survival of photoreceptor cells in the retina and sensory hair cells in the inner ear. Genetic mutations in the *USH2A* gene, which encodes usherin protein, are the most common cause of Usher syndrome worldwide, with *c.2299delG* (p.Glu767Serfs*21) being the most frequent pathogenic variant. An investigational antisense oligonucleotide (ASO) for *USH2A c.2299delG*, QR-421a, designed to bypass the mutation, has already shown promise in Phase 1/2 clinical trials (Dulla et al., 2021). While recently developed chemistry provides longer ASO half-lives, repeated injection of ASOs may be required to provide long-term efficiency. To overcome this limitation, we screened novel *USH2A* exon 13 skippers and 20 AAV capsids with the goal of developing a vectorized ASO exon skipping strategy. Optimized vectors and skippers were evaluated in inner ear and retinal organoids derived from human stem cell lines bearing the *USH2A c.2299delG* mutation. The data revealed enhanced skipping of the pathogenic exon, offering an alternative strategy for treatment of USH2A patients using a single local injection which may prevent progression of vision and hearing loss.

INTRODUCTION

Usher (USH) syndrome is associated with combined loss of vision and hearing. Clinically, USH syndrome is divided into four clinical subtypes according to the onset and severity of the symptoms (Velde et al., 2022). Each subtype is associated with mutations in different sets of genes, all expressed in sensory hair cells of the inner ear, and the photoreceptor cells of the retina. USH genes encode distinct proteins that play structural and functional roles essential for development, maturation, maintenance and sensory function in hair cells and photoreceptors as well as synaptogenesis between sensory cells and afferent neurons. The most common form of USH in the United States, Europe, and Asia is USH2A (Bonnet et al., 2011; Besnard et al., 2012; Aparisi et al., 2014; Karali et al., 2022; Li et al., 2022). *USH2A* is associated with disruptions in expression of a large protein called Usherin. While its precise role in hair cells and photoreceptor cells remains unclear, Usherin appears to be essential for the development or maintenance of these sensory cells. There are two Usherin transcripts: a short isoform (isoform A, 170 kDa), which is secreted and encoded by 21 exons, and a long isoform (isoform B, 580 kDa), which includes a transmembrane domain and is encoded by 72 exons. The most common ancestral mutation in *USH2A* is a point deletion in exon 1*3 (c.2299delG),* resulting in a frameshift and stop codon (p.Glu767Serfs*21) (Yan et al., 2009; Carss et al., 2017; Dreyer et al 2000, Meunier et al 2022).

While adeno-associated viral (AAV) gene replacement therapies have been successfully developed to target *USH* genes associated with hearing, balance, and vision loss (Pan et al., 2017; Isgrig et al., 2017; Dulon et al., 2018; Lau et al., 2023; Riaz et al., 2023), this approach is not feasible for *USH2A,* as its coding sequence exceeds 15.6 kb – significantly larger than the 4.7 kb capacity of AAV vectors. Alternatively, RNA therapies that modify RNA splicing using small antisense oligonucleotides (ASOs) may offer a viable treatment option. ASOs are short, typically 15-25 nucleotides in length, single-stranded oligonucleotides that are chemically modified to increase resistance to degradation and to enhance cellular uptake. They can be designed to alter splicing at the pre-mRNA level, an approach recently validated for *USH2A c.2299delG* (Dulla et al., 2021). Specifically, Dulla et al. (2021) developed ASOs targeting exon 13 to induce exon skipping, yielding a shorter but functional protein. This approach was subsequently brough to the clinic as Ultevursen (QR-421a) in a Phase 1/2 trial by ProQR

Therapeutics. The trial was a randomized, sham-controlled, single ascending dose study, which involved multiple centers over 24 months. Ultevursen was shown to be well-tolerated and led to improvements in visual acuity, visual field, and optical coherence. While there were plans to advance the product to a Phase 2/3 trial, the study was terminated in 2022. The study has recently restarted under a different umbrella (Thea Pharma) as a Phase 2b trial in a multicenter, double masked, randomized and sham-controlled study which aims to enroll 81 subjects (NCT06627179).

ASOs offer many other advantages: they are easily manufactured, with many already FDA-approved. They are also relatively inexpensive, capable of targeting genes of any size and lipophilic for a rapid distribution. However, ASOs are degraded by endo- and exonucleases and require repeated injections for sustained expression, which can potentially lead to toxicity over time. To address this challenge, we took advantage of U7 small nuclear RNA (snRNA). Unlike other U-rich snRNA complexes involved in pre-mRNA splicing, U7 snRNA mediates the processing of the 3′ end of histone pre-mRNAs. U7 snRNA contains three distinct functional domains: (1) the 5′ region, which includes the histone downstream element (HDE) sequence that specifically binds histone pre-mRNAs; (2) the Sm binding site, located just downstream of the 5′ region, which recruits Sm proteins essential for histone pre-mRNA processing; and (3) a 3′ stem-loop that stabilizes the structure against nuclease activity. By replacing the endogenous HDE sequence by the ASO sequence of interest and by modifying the Sm binding site to an optimized version (SmOPT) to avoid interfere with the endogenous function of the U7 snRNA, we developed an effective gene therapy tool. In addition to reducing degradation, when delivered by a viral vector, the modified U7 snRNA accumulates in the nucleus and ensures long-term expression of the ASOs, allowing for sustained clinical outcomes (Gadgil and Raczynska, 2021). This approach has been used to induce exon skipping or inclusion (Suarez-Herrera et al., 2024) and has demonstrated promising outcomes in preclinical and clinical trials for multiple diseases (reviewed in Gadgil and Raczynska, 2021).

Although, challenges related to delivery methods and toxicity may limit clinical translation of ASO therapies, Viral-based delivery methods, specifically AAV vectors, may circumvent these limitations allowing treatment of various diseases. AAVs can effectively target specific cell types, such as post-mitotic hair cells and photoreceptor

cells affected in USH syndrome. Consequently, hair cells and photoreceptors transduced by AAV vectors may express the therapeutic payload for extended periods, potentially lasting a lifetime. In this study, we report an enhanced ASO strategy combined with U7 snRNA and delivered by AAV vectors. The goal is to enhance sustained protection of hearing and vision in USH2A patients by skipping pathogenic mutations in exon 13.

RESULTS

Development of Ush2a mouse models

Two novel *Ush2a* mouse models were generated using CRISPR/Cas9 and three gRNAs to alter exon 12 sequence (equivalent to exon 13 in human) and mimic the most common frame shift mutation described in USH2A patients, i.e., *c.2299delG*.

The first mouse line, *B6-Ush2atm1BCH, referred to as* $Ush2a^{KO-1}$, has one base pair (bp) insertion leading to a premature stop codon in exon 12, followed by two large deletions (11 bp and 86 bp) in the same exon (Figure 1A). This indel is predicted to lead to expression of a truncated Ush2a protein (usherin) containing 772 amino acids (AA) instead of 5193 AA for the full-length wild-type (WT) protein. The second mouse line, *B6-Ush2atm6BCH*, named as $Ush2a^{KO-2}$ in our manuscript, presents a large deletion (331 bp) in exon 12. Similarly, this out-of-frame mutation leads to a premature stop codon and the synthesis of a truncated Ush2a protein (758 AA) (Figure S1A). Since C57BL6 mice typically carry the *Ahl* allele ($Cdh23^{753A>G}$), which is associated with progressive hearing loss (Johnson et al., 2017), both *Ush2a* knockout mouse lines were backcrossed to C57BL6J mice that were homozygous for the WT *Cdh23* allele.

No hearing phenotype in Ush2a knockout mouse lines

We evaluated the auditory function in $Ush2a^{KO-1}$ mice with analysis of broad-band click-evoked auditory brainstem responses (ABRs) between 4 and 42 weeks of age (Figure 1B-D, Table S1*).* At early time point (4 weeks), we found ABR thresholds similar to WT mice in heterozygous control ($Ush2a^{+/KO-1}$) and homozygous mutant mice ($Ush2a^{KO-1/KO-1}$). Similar results were obtained at 16 and 42 weeks of age (Table S1). Auditory tests

were also performed in response to pure tones, at frequencies ranging from 5.6 to 32.0 kHz (Figure 1E-G, Table S1). At all timepoints assessed, no statistically significant differences were observed between the control and mutant mice. Outer hair cell (OHC) function was assessed by recording distortion products otoacoustic emissions (DPOAEs) and also was not altered in homozygous *Ush2a*$^{KO-1}$ mice compared to controls (Figure 1H-J, Table S2). To determine if afferent fibers innervating the inner hair cells (IHCs) were altered in the *Ush2a*$^{KO-1}$ mutants, we analyzed the amplitude and latency of the wave 1 response at 4 and 16 weeks of age from control and *Ush2a*$^{KO-1}$ mice (Figure 1K-M, Table S3*).* No statistically significant changes were observed between the *Ush2a* $^{KO-1}$ and control mice. In addition, mechanosensory transduction currents were recorded in neonatal homozygous *Ush2a*$^{KO-1}$ mice (Figure S2, Table S5), with no deficits identified. Similar results were obtained from the second mutant line, *Ush2a*$^{KO-2}$*,* with no detectable hearing phenotype (Figure S1B-G, Table S4).

To analyze the morphology and the organization of the inner ear epithelia in *Ush2a* $^{KO-1}$ mice, the organ of Corti was dissected, fixed, and stained with phalloidin. No gross abnormality was observed in the homozygous *Ush2a* $^{KO-1}$ compared to the controls. There was no hair cell loss, no disorganization of the sensory epithelium, and hair cell stereocilia appeared well-preserved at 16 weeks of age (Figure 2A). A similar result was obtained in *Ush2a* $^{KO-2}$ mice (data not shown). As such, we conclude, based on data from two different *Ush2a*^{KO} mouse lines, that disruption of exon 12 in the mouse *Ush2a* gene does not alter auditory function, a surprising result given the prominent hearing loss phenotype of human USH2A patients bearing the similar mutations in exon 13.

Endogenous exon skipping in Ush2a mice, human inner ear (IEOs) and human retinal organoids (ROs)

To explain the lack of phenotype in *Ush2a* mouse models, we hypothesized that there may be endogenous in-frame exon 12-skipping that maintains usherin expression and normal auditory function. To evaluate this possibility, we analyzed RNA transcripts in inner ears and eyes of *Ush2a*$^{KO-1}$ mice. We harvested and snap froze cochleas and eye bulbs of mutant and WT control mice at post-natal day (P) 5-6. After extraction of total RNA, RT-PCR was used to amplify the region between exons 10 and 15. Analysis of inner ear tissue from WT control mice showed that two of the three harvested samples expressed the full-length form of *Ush2a,* as well as an alternative splice form corresponding to total skipping of exon 12. In one of three samples, a partial deletion of

the exon 12 was present, along with the full-length form of *Ush2a* (Figure 2B). The same analysis performed on cochlear tissues from *Ush2a*$^{KO-1}$ mice identified total exon 12 skipping in one out of three samples and partial exon 12 skipping in another sample (Figure 2B). In the eye tissues, no exon 12 skipping was detected in four WT mice, whereas exon 12 skipping was observed in two out of three *Ush2a*$^{KO-1}$ mice (Figure 2C). Despite variability in endogenous exon 12 skipping in both inner ears and eyes, a portion of the *Ush2a* transcripts from *Ush2a*$^{KO-1}$ mice remained in-frame. A similar result was observed in *Ush2a*$^{KO-2}$ mice that carry a larger deletion of exon 12 (data not shown).

To explore this further, we utilized organoid models derived from human induced pluripotent stem cells (iPSCs) to evaluate whether endogenous exon 13 skipping also occurred in this context. For this purpose, we used the SOX2-GFP iPSC line (Roberts et al., 2017) as the control and introduced the *USH2A* mutation (*c.2299delG*) into exon 13 using CRISPR/Cas9 (Synthego). Using these cell lines, we generated human inner ear organoids (IEOs) and retinal organoids (ROs) from both the healthy control (IEO^{SOX2}/RO^{SOX2}) and *c.2299delG* mutant (IEO^{C20}/RO^{C20}) iPSC lines. Notably, prior studies have established that hair cells in IEOs and photoreceptors in ROs express *USH2A*. Hair cells can be identified in IEOs around D40 (Koehler et. al., 2017, Steinhart et.al., 2023, van de Valk et.al., 2023). In ROs, the photoreceptor outer segment, containing precursor photoreceptor cells, becomes visible after D120 (Afanasyeva et al. 2021*)*. Functional photoreceptors are typically identified by D220 (Figure 3A). We assessed exon skipping at three different time points in both organoid models: D106, D118 and D141 in IEOs, and D128, D162 and D183 in ROs. In IEO^{SOX2}, alternative splicing was detectable only at the latest time point (D141), showing in-frame endogenous exon 13 skipping and out-of-frame dual exon 12 & 13 skipping (Figure 3B, left). Additionally, we also observed alternative splicing at early stages, with variability between samples from the same culture (Figure S3), similar to what was previously noted in mouse tissue. In mutant IEO^{C20}, both endogenous exon 13 and dual exon 12 & 13 skipping were observed at D141 (Figure 3B, right). In control ROs, different results were obtained, with no exon 13 skipping detected; however, dual exon 12 & 13 skipped transcripts were observed in most control RO^{SOX2} samples at all stages (Figure 3C, left). In contrast, mutant RO^{C20} samples contained *USH2A* transcripts with in-frame exon 13 skipping and out-of-frame dual exon 12 & 13 skipping across all tested samples (Figure 3C, right). We observed an increase in alternative transcripts

as the organoids matured and an increase in exon 13 skipping associated with the presence of the single base pair deletion. These findings suggest that the single base pair deletion in *USH2A* promotes endogenous exon 13 skipping in mutant cells lines.

Generation of USH2A reporter and screening of exon 13 skippers

Given the level of endogenous exon skipping in mouse inner ear and retina and in human organoids, we sought to develop an *USH2A* reporter construct to facilitate screening ASOs that may further enhance exon 13 skipping. We generated an eGFP reporter construct containing human *USH2A* exons 12-14, along with their respective introns, incorporating the human exon 13 *c.2299delG* mutation (*USH2A* exon 12 - intron 12 - exon 13 (*c.2299delG*) - intron 13 - exon 14 - P2A - eGFP). The construct was designed so that GFP would only be expressed when the reading frame is restored, i.e., when *USH2A* exon 13 is skipped (Figure 4A). Next, we generated a stable cell line by transfecting HEK293 cells with the USH2A-eGFP reporter plasmid and selected for increased eGFP signal after transiently transfecting the U7 snRNA skipper construct encoding QR-421a antisense sequence from Dulla et al. (2021; pU7-USH2A-Ex13-snRNA-QR-421a).

To screen ASO sequences we generated more than 600 U7 snRNA skippers targeting the entire region of exon 13 and its intron-exon boundaries (Table 1). As a positive control we also used the U7 snRNA skipper construct encoding the QR-421a antisense sequence (pU7-USH2A-Ex13-snRNA-QR-421a) and we used a non-hybridizing sequence as a negative control.

Cells expressing the USH2A-eGFP reporter construct were plated in 96 well plates and transiently transfected with the U7 snRNA skippers specific to exon 13. eGFP signal was measured with ImageXpress Micro Confocal high content imager (Figure 4B). The skipper efficiency was assessed based on the increase in GFP signal. GFP signal values from *USH2A* exon 13 U7 snRNA skippers were normalized to the GFP signal of the positive control, U7 snRNA QR-421a. Approximately 100 U7 snRNA skippers showed higher GFP signals (>1.5-fold) compared to U7 snRNA QR-421a. Notably, several U7 snRNA skippers outperformed U7 snRNA QR-421a for more than 2.5-fold increase in GFP signal (Figure 4C).

Combinations of several efficient skipper sequences were linked in tandem and delivered by a single U7 snRNA molecule (U7 snRNA dual skipper) and were evaluated relative to the efficiency of individual antisense skippers. Some U7 snRNA dual skippers showed greater efficacy than individual antisense sequences. For example, dual skipper 4+7 performed much better than individual skipper 4 or skipper 7 (Figure 4D). The dual skipper sequence with strongest GFP expression (4+7) was packaged into AAV vectors for further testing.

Assessment of AAV capsids for targeting inner ear tissue

We previously demonstrated that the AAV9-PHP.B capsid exhibits high efficiency in targeting inner ear tissue (Lee et al., 2020; Wu et al., 2021). To investigate whether new capsids across related as well as diverse clades could enhance gene expression, we tested twenty distinct AAV capsids encoding GFP under a CMV promoter. For testing, we injected the vectors into the inner ears of WT mice between P1 and P2 (Figure 5A). Ten days post injection, the injected inner ears were harvested and processed for confocal imaging. The percentage of GFP-positive cells was quantified by blinded investigators to compare the efficiency of each capsid. Of the twenty capsids examined, only eight (capsids 1, 5, 12, 13, 14, 17, 18, and 20) exhibited GFP expression in cochlear hair cells, albeit with lower expression levels compared to AAV9-PHP.B (Figure 5B-C & Figures S4-5). Notably, five capsids primarily targeted supporting cells (capsids 2, 3, 4, 5 and 6), while four capsids predominantly targeted spiral ganglion neurons (capsids 3, 4, 6, and 9). Most of the tested capsids either did not infect the inner ear tissue or did so at a very low level (capsids 7, 8, 10, 11, 15, 16, and 19) (Figure 5B-C & Figures S4-5). Although some novel capsids showed noteworthy properties for targeting neurons and supporting cells. AAV9-PHP.B (capsid 1) remained the most efficient capsid for targeting auditory hair cells, infecting an average of 91% of inner hair cells (IHCs) and 54% of outer hair cells (OHCs) along the tonotopic axis (Figure 5B-C & Figure 6). Additionally, AAV9-PHP.eB (capsid 20) and Bpo.394 (capsid 17) demonstrated notable efficiency, infecting approximately 61% and 45% of IHCs and around 30% and 25% of OHCs, respectively, along the tonotopic axis (Figure 5B-C & Figure 6). Interestingly, for these two capsids, an inverse gradient was observed along the tonotopic axis, with more IHCs infected at the apex and more OHCs infected at the base.

Assessment of vectorized antisense skippers in organoids

We packaged the most promising U7-skippers (dual skipper 4+7) into AAV9-PHP.B capsids along with the coding sequence for the transfection marker, mKate, driven by a CMV promoter (AAV9-PHP.B-skipper-mKate). The efficiency of the validated AAV9-PHP.B-skipper-mKate was first tested on IEOs (Figure 7A-C). To enhance viral uptake, organoids were sliced and splayed open to expose hair cells and the virus was bath-applied. After 14-16 days of incubation, we confirmed the specific viral infection of organoid hair cells through immunostaining and live-cell imaging (Figure 7C, Video S1-2). Total RNA was extracted from each condition, followed by transcriptomic analysis through RT-PCR. First, we tested the efficiency of the skipper in early (D 79-87) control IEOs (IEO^{SOX2}). Consistent with prior data, endogenous exon 13 skipping was detected in IEO^{SOX2} samples that were not exposed to the skipper (Figure 7D, S3). However, endogenous skipping was only present in some samples and at a low level. On the other hand, in organoids exposed to AAV9-PHP.B-skipper-mKate, the level of exon 13 skipping increased (Figure 7D, S3). Similarly, an increase of dual exon 12 & 13 skipping, which leads to an out of frame transcript and a truncated protein, was also present in all conditions that received the virus.

Encouraged by these results, we decided to target organoids at different developmental stages in both control (IEO^{SOX2}) and mutant (IEO^{C20}) organoids. As controls, we used AAV9-PHP.B-mKate without skippers (AAV9-PHP.B-mKate-empty). In the same way, we applied the virus directly into the culture media, and after 14-16 days of incubation, we performed the transcript analysis. In control organoids (IEO^{SOX2}), across all ages tested (from D106 to D141), a substantial increase in exon 13 skipping was observed in response to the AAV9-PHP.B-skipper-mKate (Figure 7E-F). Little exon 13 skipping was detected in both control conditions (AAV9-PHP.B-mKate-empty and no virus), except at older stages (D141), where it was similar to the level of endogenous exon 13 skipping. The level of exon 13 skipping in IEO^{SOX2} treated with the AAV9-PHP.B-skipper-mKate was elevated by 5.6-fold and 10.9-fold (n = 3) compared to the control condition (AAV9-PHP.B-mKate-empty) and untreated condition, respectively (Table S6). Similarly, IEO^{C20} showed an 8.2-fold and 8.7-fold (n = 3) higher level of exon 13 skipping in response to the AAV9-PHP.B-skipper-mKate versus the control condition (AAV9-PHP.B-mKate-empty) and untreated condition, respectively (Table S6). Together, the data demonstrate that the application of AAV9-PHP.B-skipper-mKate substantially increased exon 13 skipping in IEOs.

Motivated by reports that showed efficient viral transduction in the inner ear and retina using AAV2-7m8 capsids (Dalkara et al., 2013; Isgrig et al., 2019; Lee et al., 2020), we package the U7-skippers (dual skipper 4+7) into the AAV2-7m8 capsids along with the coding sequence for the transfection marker, mKate driven by a CMV promoter (AAV2-7m8-skipper-mKate). As controls, we used AAV2-7m8-GFP without skippers (AAV2-7m8-GFP-empty). As with the previous experiments, the AAV2-7m8 vectors were applied directly into the culture media, and after 14-16 days of incubation, we performed the transcript analysis. In control organoids (IEO^{SOX2}), at D67 and D73, a significant increase in exon 13 skipping was observed in response to the AAV2-7m8-skipper-mKate (Figure 7G-H). Exon 13 skipping in IEO^{SOX2} treated with the AAV2-7m8-skipper-mKate was elevated by 17.9-fold and 24.8-fold (n = 4) compared to organoids exposed to AAV2-7m8-GFP-empty and untreated condition, respectively (Table S6). Similarly, mutant IEO^{C20} showed a 40.6-fold and 12.9-fold (n = 4) higher level of exon 13 skipping in response to the AAV2-7m8-skipper-mKate versus the control condition (AAV2-7m8-GFP-empty) and untreated condition, respectively (Table S6). These results show that AAV2-7m8-skipper-mKate efficiently enhanced exon 13 skipping in IEOs. By using AAV2-7m8 capsid, we efficiently targeted organoid hair cells as evident from mKate and GFP expression (Figure 7I). Overall, the AAV2-7m8 capsid led to greater exon 13 skipping efficiency than the AAV9-PHP.B capsid.

Unlike IEOs, endogenous dual exon 12 & 13 skipping was present in most all RO conditions and cell lines tested (RO^{SOX2} and RO^{C20}) (Figure 3C). Additionally, no obvious change in exon 13 skipping was observed in RO^{SOX2} and RO^{C20} treated with AAV9-PHP.B-skipper-mKate (Figure 8A-E, Table S7). We attributed this result to differences in endogenous exon skipping and insufficient viral transduction of photoreceptor cells using this vector. Indeed, we observed little mKate expression in ROs, suggesting that the AAV9-PHP.B viral capsid was less effective in transducing these organoids (Figure 8C, S7, Video S1-2). We therefore decided to assess exon skipping efficacy using a different viral vector. Previous reports have shown that the AAV2-7m8 capsid can efficiently transduce retinal cells (Dalkara et al., 2013) and retinal organoids (Garita-Hernandez et al., 2020). As such we used U7-skippers (dual skipper 4+7) packaged into AAV2-7m8 capsids. Using the protocol used previously, we applied the AAV2-7m8 vectors directly into culture media bathing ROs, and after 14-16 days of incubation, we performed the transcript analysis. At D105, control organoids (RO^{SOX2}) showed a significant increase

in exon 13 skipping in response to the AAV2-7m8-skipper-mKate (Figure 8F-H, Table S7, *n* = 6). No exon 13 skipping was detected in both control conditions (AAV2-7m8-GFP-empty and no virus). In mutant organoids (RO^{C20}), we observed a significant increase in exon 13 skipping in response to the AAV2-7m8-skipper-mKate (Figure 8F-H, Table S7). The level of exon 13 skipping in RO^{C20} treated with the AAV2-7m8-skipper-mKate was elevated 92-fold and 71-fold (*n* = 6) compared to the control condition (AAV2-7m8-GFP-empty) and untreated condition, respectively (Table S7). In summary, we found that the AAV2-7m8 skippers were able to transduce organoid photoreceptor cells (Figure 8H, Table S7) and yielded high skipping efficiency.

DISCUSSION

Viral gene replacement therapies have been developed for several genetic disorders of the retina, and recently, for hearing loss due to mutations in otoferlin (*OTOF*), which has a coding sequence too large to be delivered by single AAV vectors. Clinical trials evaluating dual vector *OTOF* gene replacement are currently ongoing in the U.S., Europe and China with encouraging preliminary data, demonstrating both safety and efficacy (Wang et al., 2024; Qi et al., 2024). Moreover, the eye and the ear are unique in that they provide immune-privileged environments, are accessible for local injection, and possess mature, post-mitotic sensory cells, making them attractive targets for viral gene replacement therapies. However, the large size of some coding sequences, such as *USH2A* (>15 kB), poses a major challenge for gene replacement therapies, as they exceed the capacity of AAV (~4.7 kB) and lentiviral vectors (~8 kB), making viral-based gene delivery impractical.

Alternate strategies for treating *USH2A* mutations have been developed based on antisense oligonucleotides (ASOs). Over the past decade, ASO therapies have been designed that target mutations in several *USH* genes, including *USH1C* (Lentz et al., 2013; Lentz et al., 2020), *USH3A* (*CLRN1*; Panagiotopoulos et al., 2020), and *USH2A* (Slijkerman et al., 2016; Dulla et al., 2021). These ASO therapies have targeted cryptic splice sites, intronic mutations, and mutated exons. Pendse et al. (2019) validated functional preservation after exon 12 deletion in a novel *Ush2a* knock-in mouse model, while Dulla et al. (2021) validated this approach in *Ush2a* zebrafish models. These reports have provided a solid foundation for developing ASO strategies to treat

prevalent *USH2A* mutations. Unfortunately, ASO therapies also face a major challenge: limited durability, because they are susceptible to degradation by endo- and exonucleases. As such, ASOs may necessitate repeated injections to maintain therapeutic efficacy.

To circumvent the limited durability of ASOs and the limited capacity of viral gene replacement, we designed a novel strategy that merges efficient AAV viral delivery with targeted ASO sequences into a single therapeutic strategy, designed to restore *USH2A* expression. U7 snRNAs can be modified to encode ASO sequences, and when packaged into viral vectors, can provide prolonged expression of the ASO, thereby enabling long-term therapeutic benefit. While this approach has not been applied in the field of hearing and vision restoration, the U7 snRNA antisense system has been validated for treatment of other human diseases, including Duchenne muscular dystrophy (DMD) and spinal muscular atrophy (SMA) (reviewed in Lesman et al., 2021). Another important advantage of this approach is that AAV vectors can be used to deliver multiple ASO sequences thereby allowing multiple splicing defects to be targeted in one or more genes.

As such, we screened 20 AAV capsids and identified efficient AAV vectors for targeting sensory hair cells. In parallel we screened over 600 ASO sequences and identified a dual ASO combination that maximized exon 13 skipping, which carries the most common pathogenic *USH2A* mutation (*c.2299delG*). The dual skipper sequences were packaged as U7 snRNAs into AAV9-PHP.B and AAV2-7m8 capsids. The goal of this approach was to restore expression of an in-frame *USH2A* transcript that lacks exon 13. We demonstrated improved skipping efficiency with novel antisense sequences and validated the application of vectorized ASOs *in vitro* in IEOs and ROs derived from human iPSCs bearing the *c.2299delG* mutation in exon 13 of *USH2A*.

Unfortunately, the development of effective therapies for USH2A patients has been hampered by the lack of mouse models that replicate the human phenotype. Several research teams developed *Ush2a* mouse models that failed to mimic USH2A patient phenotypes. Disruption in *Ush2a* expression in mice is associated with photoreceptor degeneration and decline in retinal function (Liu et al., 2007; Tebbe et al., 2023). However, most of these models fail to recapitulate the hearing phenotype of USH2A patients. The mouse models show little to no

hearing loss depending on the genetic background. One recently developed mouse model (Crane et al., 2023) demonstrated mild hearing loss at low frequencies, which differs from the hearing profile of USH2A patients, who typically have hearing loss that progresses over time beginning at the high frequency end of the auditory spectrum (Liu et al., 2007; Zou et al., 2015). Consistent with prior reports, the two novel *Ush2a* mouse models developed for this project (*Ush2a*$^{KO-1}$ and *Ush2a*$^{KO-2}$) also had normal auditory thresholds. We hypothesize that the lack of phenotype in *Ush2a* exon 12 mouse models (equivalent to exon 13 in humans) may be due to the presence of endogenous in-frame exon 12 skipping that preserves the function Usherin protein. We further speculate that similar endogenous skipping may contribute to variability among USH2A patients harboring the equivalent exon 13 mutation. Endogenous skipping may also contribute to variability in the progression of the disease between ears and eyes, with vision loss progressing more slowly than hearing loss in human USH2A patients. This hypothesis is supported by the presence of alternative transcripts identified in nasal epithelial cells from USH2A patients carrying the *c.2299delG* mutation (Lenassi et al., 2014). Using RT-PCR, Lenassi et al. (2014) demonstrated expression of *USH2A* transcripts lacking exon 13 (exon 12 in mouse) or exon 12 and 13 (exons 11 and 12 in mouse). Bioinformatic analysis suggests that the single base pair deletion in exon 13 (*c.2299delG*) disrupts cis-regulatory elements, leading to the generation of new alternative splicing patterns. Consequently, the mutation has been shown to result in altered RNA splicing, particularly exon 13 skipping. Interestingly, and consistent with our findings in mouse tissue and human organoids, this effect was variable and observed in some, but not all, patients harboring the same mutation. In contrast to human nasal epithelial cells, we found that some WT control mice and some control human organoids also had in-frame transcripts lacking exon 12 or 13, respectively. The mechanisms and factors that contribute to the variability of endogenous exon skipping are not clear but are worthy of further investigation. If the native splicing mechanisms can be manipulated to induce greater levels and greater consistency of exon 13 skipping, they may provide a novel strategy for therapeutic development.

Although other USH2A animal models, such as zebrafish and rabbits, have visual and hearing impairment phenotypes, more similar to those of USH2A patients (Dona et al., 2018; Dulla et al. 2021; Nguyen et al., 2023), we opted to focus on 3D organoids derived from human iPSCs, which provide a robust platform for testing sequence-specific therapeutic approaches for USH2A patients (Sanjurjo-Soriano et al., 2023). Protocols have been

developed that enable generation of both IEOs and ROs (Koehler et. al., 2017; Steinhart et.al., 2023; van de Valk et.al., 2023). These organoids can be generated from control human iPSC lines, patient-derived iPSCs, or genetically modified iPSC lines. For this project, we generated human IEOs and ROs from control iPSCs and iPSCs that were genetically edited to carry the human *c.2299delG USH2A* mutation. We determined use of exon 13 in these organoids with and without vectorized ASO treatment. While the organoid models provided a powerful platform for evaluating the efficacy of vectorized ASOs, they did not allow for physiological assays for restoration cellular function because no functional deficits were apparent in the mutant organoids. In human USH2A patients and in *Ush2a* mouse models, hearing and vision deficits do not develop until postnatal and adult stages, respectively, whereas the organoids used for this study were aged to day 183 *in vitro*, equivalent to late 2nd trimester of human fetal development. However, because organoid hair cells and photoreceptors expressed *USH2A* at early stages, they were useful models for evaluating vector targeting and exon skipping.

As such, we used both inner ear and retinal organoids to investigate U7 snRNA technology to vectorize potent ASO sequences to target sensory hair cells and photoreceptors. Through a systematic walk-through technique along exon 13 of *USH2A*, we identified ASO sequences with high efficiency. Testing this vector-based construct on human IEOs and ROs carrying the common human *USH2A* exon 13 mutation, *c.2299delG*, resulted in a significant increase in exon 13 skipping in IEOs and ROs. The endogenous exon 12 / 13 skipping in mouse and human, respectively, bodes well for the therapeutic exon skipping approach. Since the native tissue may be predisposed to exon 12 / 13 skipping, introduction of antisense sequences that target *USH2A* splice sites in this region may further enhance exon skipping, thereby increasing the therapeutic benefit.

We did not see evidence of enhanced skipping of exon 13 in ROs using AAV9-PHP.B-skipper-mKate. We suspect this was a consequence of limited viral transduction of RO photoreceptor cells. While we performed a large capsid screen that identified AAV9-PHP.B as an effective capsid targeting sensory hair cells in the mouse inner ear, we observed little mKate expression in ROs, suggesting that our batch of AAV9-PHP.B-skipper-mKate was less efficient at targeting RO photoreceptors. However, a publication from Ivanchenko et al. (2023) demonstrated efficient transduction of human RO photoreceptor cells using the AAV9-PHP.B capsid. In addition, Muller et al.

(2025) recently showed that the AAV9-PHP.B capsid efficiently targets photoreceptors of native human retinas as well, suggesting the AAV9-PHP.B capsid may be well-suited for clinical application.

Alternatively, we found that the AAV2-7m8 capsid allowed efficient targeting of human organoid hair cells and photoreceptors and promoted a substantial increase in exon 13 skipping in both control and mutant organoids. Use of a vectorized ASO with a viral capsid that transduces native human hair cells and photoreceptors would be advantageous as it would support local delivery of a single therapeutic construct into both sets of sensory tissues. One time delivery of a single therapy that preserves or restores function in both eyes and ears would provide meaningful improvement in quality of life for USH2A patients. Given the normal auditory function in our mouse lines harboring *Ush2a* exon 12 mutations, the endogenous exon 12 skipping in mice, endogenous exon 13 skipping human organoids and the Dulla et al. (2021) data showing normal auditory and visual function in zebrafish lacking exon 13, strong evidence now supports that the corresponding region of the USH2A protein is dispensable, increasing the therapeutic potential of the exon 13 skipping strategy to treat the most common Usher syndrome mutation, *USH2A* c.2299delG. Lastly, we suggest that vectorized delivery of ASO sequences could be developed to target other mutations in USH2A, other large USH genes, such as ADGRV1 (USH2C) and MYO7A (USH1B) and could include multiple ASO sequences, to promote skipping of multiple exons and restoration of protein function.

MATERIALS and METHODS

Mice

All animal experiments were performed in accordance with the NIH guidelines and were approved by the Institutional Animal Care and Use Committee (protocols #20-02-4149R and #00001240) at Boston Children's Hospital. C57Bl/6J mice from Jackson Laboratories (Bar Harbor, ME, USA) were used for our experiments. Additionally, two *Ush2a* mouse models for the human exon 13 mutation were generated by the BCH Gene Manipulation Core facility using CRISPR/Cas9 and a combination of three guide RNAs. The first line was created with two different guide RNA targeting *Ush2a* exon 12 (5'- TAAGGTGTGACAAGTCAACC GGG -3' and 5'-

CAACTCTGTGATCCGCTTTC TGG -3'). *Ush2a*$^{KO-1}$ possess 1 base pair (bp) insertion and 2 large deletions (11 and 86 bp) into exon 12. The second line *Ush2a*$^{KO-2}$ presents a large deletion (331bp) into the exon 12 of *Ush2a* generated by the Cas9 with two guide RNAs (gRNAs) that specifically target the exon 12 of *Ush2a* gene (5'-GGACAATCCTCAAGGTTGTC AGG-3' and 5'- CAACTCTGTGATCCGCTTTC TGG -3'). The mutant mouse lines were backcrossed to *Cadherin 23 (Ahl)* corrected lines to remove the mutation (*c.753A>G*) that is associated with progressive hearing loss. For the manuscript, we report work performed on *Ush2a*$^{KO-2}$ in the supplementary material, as this mouse line mimicked *Ush2a*$^{KO-1}$.

Genotyping was performed on genomic DNA (gDNA) extracted from toes or tail clips using DirectPCR lysis reagent (ear) (Viagen Biotech, #402E, Los Angeles, CA, USA) supplemented with proteinase K (New England Biolabs, #P8107S, Ipswich, MA, USA). Polymerase Chain Reaction (PCR) were performed using GoTaq® Master Mix (Promega, #M7122, Madison, WI, USA) and primer sets included in *Table S8*. For the *Ush2a* genotyping, the PCR reaction was run in a thermocycler programmed for 95 °C for 5 min, [95 °C for 30 sec, 50 °C for 1 min, 72 °C for 2 min] × 35 cycles, 72 °C for 5 min, and then maintained at 4 °C until further analysis. For the *Ahl* genotyping, the PCR reaction was run in a thermocycler programmed for 94 °C for 5 min [94 °C for 15 sec, 64 °C for 30 sec, 72 °C for 30 sec] × 30 cycles, 72 °C for 7 min, and then maintained at 4 °C until further analysis. The iBright CL1500 imaging system (Invitrogen) was used to visualize amplicon bands on 1-2% agarose gel. The band of interest was extracted and purified from the agarose gel using Monarch® DNA gel extraction kit (New England Biolabs, #T1020S, Ipswich, MA, USA). The mutation was confirmed by Sanger sequencing using Genewiz platform.

Mice of both sexes were used in equal proportion. All mice were kept in a 12 hr light/12 hr dark cycle with accessibility to food and water *ad libitum*. Tissue collection was performed immediately post-mortem. At least three animals per group were used for each experiment.

Auditory Brainstem Responses (ABR) and Distortion Product Otoacoustic Emissions (DPOAE)

ABRs and DPOAEs recordings were performed on heterozygotes *Ush2a*$^{+/KO-1}$ and *Ush2a*$^{+/KO-2}$, used as controls, and homozygotes *Ush2a*$^{KO-1/KO-1}$ and *Ush2a*$^{KO-2/KO-2}$ mice at 4, 16, and 42 weeks old. Mice were anesthetized by intraperitoneal injection with a mix of ketamine (100 mg/kg) and xylazine (15 mg/kg) diluted into saline solution. Mice were maintained anesthetized on a heating pad inside a sound-proof chamber. Three electrodes were inserted subcutaneously, (1) the reference electrode is inserted at the vertex of the skull between the two ears, (2) the recording electrode were inserted behind the left pinna, and the ground electrode were inserted along the rear left leg. To expose the ear canal, the meatus at the base of the pinna was resected. Then, the speaker/microphone apparatus was inserted at the entrance of the ear canal. To validate the proper positioning of the apparatus, the system was calibrated for each mouse prior to any recording.

For ABRs, acoustic stimuli of 5.6, 8.0, 11.3, 16.0, 22.6 and 32.0 kHz consisted of 5 ms tone bursts and were presented to the mice at 5 decibels (dB) steps from 10 to 90 dB sound-pressure level (SPL). ABR responses were amplified (10,000 times), filtered (0.1 to 3 kHz), averaged (at least 512 times) with stimuli polarity alternated after 'artefact rejection' and digitized on EPL software (EPL Acoustic system, Mass Eye and Ear, Boston, MA, USA). The auditory threshold was visually determined and corresponds to the lowest intensity of sound leading to a detectable wave form.

For DPOAEs, the data were collected during the same session and under the same conditions. DPOAE responses were generated when the cochlea was presented to two distinct pure tones (f1 and f2). The ratio 1:2 of pure tones (f2/f1) was presented to the mouse. f2 varied between 5.6 to 42.5 kHz in half-octaves steps and a 5 dB f2 steps from 10 to 80 dB SPL for the generation of DPOAEs at 2f1-f2. DPOAE thresholds were visually determined as the f2 level required to produce DPOAEs above 0 dB. Data were plotted on GraphPad version 9 software as mean ± standard deviation (S.D.).

Electrophysiological recordings and mechanical stimulation

Recordings of mechanotransduction currents were performed as previously described (Pan et al., 2017). Briefly, whole-cell voltage-clamp recordings were performed in standard perilymph solution with borosilicate recording pipettes filled with standard high potassium intracellular solution. Mechanical stimuli were provided by a stiff glass probe mounted on a piezoelectrical actuator (Physik Instruments, Waldbronn, Germany). Data were analyzed offline with Origin (OriginPro 2021b, Origin lab corporation).

Generation of USH2A-eGFP reporter construct

A fragment of the human *USH2A* gene (NG_009497.2) containing *USH2A* exon 12 – intron 12 – exon 13 (*c.2299delG* mutation) – intron 13 – exon 14 was synthesized (Azenta, Burlington, MA) and cloned into a plasmid containing a eGFP coding sequence and a CMV promoter to create a fusion construct comprising the *USH2A* gene fragment (with *c.2299delG* mutation) in frame with eGFP-coding sequence (pCMV-USH2A-exon 13 skip eGFP reporter).

Generation of stable USH2A-eGFP reporter cell line

HEK293T cells were transfected with the pCMV-USH2A-exon 13 skip eGFP reporter plasmid. PEIpro transfection reagent (Polyplus, 115-0015, France) was used to transfect AAVPro® 293T cell line (TaKaRa, California USA). Cells were cultured for 2 weeks under puromycin selection (Mirus, MIR 5940, Wisconsin USA). to achieve a stable pool. Clonal selection was then performed by limiting dilution into 96-well plates (Corning, 3596, Arizona USA) to isolate individual stable cell clones. Stable USH2A-eFGP reporter cell clones were screened for increased GFP signal following transient transfection with 50 ng of U7 snRNA skipper construct encoding the QR-421a antisense sequence (Dulla et al. 2021). GFP signal was measured three days post-transfection in 96-well plates (Greiner Bio-One International GmbH, 655090, North Carolina USA) in 1X DPBS buffer (Corning, 21-031-CV, Arizona USA). All wells were imaged using the FITC fluorescence channel (475/34 nm) on an ImageXpress Micro Confocal high-content imager (Molecular Devices, California USA), and pixel intensity in the FITC channel was captured and quantified. The USH2A-eGFP reporter stable cell clones with the highest increased GFP signal after transfection were selected.

U7 snRNA skipper constructs

U7 snRNA skipper constructs were engineered based on the previously described U7 smOPT-SD23/BP22 construct (modified murine U7 snRNA gene) (Goyenvalle et al., 2004). The original Sm domain sequence (AATTTGTCTAG) was replaced with the optimized smOPT sequence (AATTTTTGGAG), and the native histone pre-mRNA pairing region was substituted with 619 antisense sequences specifically targeting human *USH2A* exon 13. The following skipper sequences were selected for further analysis: QR-421a: AGCTTCGGAGAAATTTAAATC (Dulla et al., 2020). Skipper 4: AGAATTTGTTCACTGAGCCATGGAGGTTAC; Skipper 7: ATTACACCTTCTTCCTTGACGATTAGGCAC; Dual skipper 4+7: AGAATTGTTCATGAGCCATGGAGGTTACATTACACCTTCTTCCTTGACGATTAGGCAC. The modified U7 snRNA skipper fragments were synthesized and subsequently cloned into the pAAV plasmid (Azenta, Burlington, MA) for packaging into viral vectors.

AAV production

All AAV vectors, with the exception of AAV2-7m8, were produced by SAB Tech Inc. by co-transfecting HEK293T cells with three plasmids: the pAAV plasmid encoding the transgene flanked by AAV inverted terminal repeats (ITRs), a rep-cap expression construct encoding the specific AAV serotype capsid, and a helper plasmid expressing adenoviral elements E2a, VA, and E4-orf6. Forty-eight hours post transfection, AAV vector particles were purified from cell lysates using cesium chloride gradient centrifugation. AAV2-7m8 vectors were generated by the Vector Core at Boston Children's Hospital, using a helper virus free system and a double transfection method. Titers were calculated by qPCR to be 1.25E+13gc/mL for the AAV2-7m8-CMV-mKate-skipper and 6.24E+12gc/ml for the AAV2-7m8-CMV-GFP-empty vectors. AAV2-7m8 vectors were purified using an iodixanol step gradient followed by ion exchange chromatography. All virus aliquots were stored at −80°C and thawed just before use.

In vivo surgery

Inner ear injections were performed according to the Institutional Animal Care and Use Committee at Boston Children's Hospital (protocols #20-02-4149R and #00001240). Wild-type (WT, C57BL6) mice were obtained from The Jackson Laboratory. Neonatal mice, at postnatal day 1 (P1) or 2 (P2), were anesthetized by hypothermia,

achieved by placing them on crushed ice for 3 min and then transferring them onto an ice pad to maintain the anestesia throughout the surgery (~10-15 min). A post-auricular incision was made to expose the semicircular canals, and a stereomicroscope (Stemi 2000, Zeiss, Germany) was used for visualization. The injection was administered through the utricle using a glass micropipette filled with 1 uL of the desired virus. Upon wound closure with sutures, mice are transferred onto a heating pad for recovery. Standard post-operative care was provided for the following 5 days.

Tissue preparation, imaging and hair cell quantification

Temporal bones were harvested at P10 and immediately fixed in 4% paraformaldehyde (PFA, #15713-S, Electron Microscopy Science, Hatfield, PA, USA) at room temperature (RT) with agitation for 1 hr. Prior to dissection, tissues were decalcified in 120 mM ethylenediaminetetraacetic acid (EDTA) for 12 to 24 hrs. The full turns of the cochlea, along with the utricle, saccule, and ampullas, were dissected. Tissues were then permeabilized with 0.5% Triton-X 100 (Sigma Aldrich, #X100-5ML, Saint Louis, MO, USA) for 1 hr at RT, followed by immunostaining with phalloidin 405 (1:500, Thermo Fisher Scientific, #A30104, Waltham, MA, USA) for 2 hrs at RT. After PBS washes, samples were mounted with Vectashield antifade mounting medium containing DAPI (Vector laboratories, #H-1200-10, Newark, CA, USA).

Images were acquired using a confocal microscope (LSM800, Zeiss, Germany), with Z-stacks captured at 0.3 µm intervals. Three-dimensional projection images were generated from Z-stacks using the open-source software Fiji. The ‘Cell Counter’ plugin in Fiji was used to quantify the total number of hair cells, identified based on phalloidin staining, as well as the total number of virus-infected, GFP-positive hair cells.

RNA extraction, Reverse Transcriptase Polymerase Chain Reaction and Quantitative RT-PCR

Temporal bones and eye bulbs were harvested from euthanized mice and immediately flash-frozen in liquid nitrogen. Total RNA was isolated using a combined Trizol/chloroform extraction protocol with PureLink RNA mini

kit (Thermo Fisher Scientific, #12183018A, Waltham, MA, USA). Similarly, retinal and inner ear organoids derived from hiPSCs were quickly harvested and flash-frozen in liquid nitrogen prior to total RNA isolation.

A Two-Step RT-PCR was performed on temporal bones and eye bulbs. According to the manufacturer's protocol, cDNA was generated by reverse transcription using the iScript™ Advanced cDNA Synthesis Kit (Qiagen, #1725037, Germany). PCR was subsequently performed with 50 ng of cDNA using the Q5® Hot Start High-Fidelity DNA Polymerase (New England Bioloabs, #M0493, Ipswich, MA, USA). The region between exons 10 and 15 of the murine *Ush2a* gene was amplified using primer sets listed in *Table S9*, with the following PCR program: 98 °C for 5 min [98 °C for 10 sec, 60 °C for 10 sec, 62 °C for 30 sec, 72 °C for 45 sec] × 40 cycles, 72 °C for 5 min, and then held at 4 °C until further analysis. PCR products (20-40 µL) were run on a 2% agarose gel. The iBright CL1500 imaging system (Invitrogen, Waltham, MA, USA) was used to visualize amplicon bands. Bands containing the gene of interest were extracted and purified from the agarose gel using the Monarch® DNA Gel Extraction Kit (New England Bioloabs, #T1020S, Ipswich, MA, USA). Sanger sequencing was performed on the extracted DNAs using the Genewiz from Azenta life sciences (South Plainfield, NJ, USA) platform to confirm sequence accuracy.

A One-Step RT-PCR was performed on inner ear organoids (IEOs) and retinal organoids (ROs) generated from human induced pluripotent stem cells (hiPSCs) using the SuperScript™ IV One-Step RT-PCR System (Thermo Fisher Scientific, #12594100, Waltham, MA, USA). The region between exons 10 and 16 of human *USH2A* (gene was amplified using primer sets listed in *Table S9*. The following PCR program was used: 50 °C for 10 min, 98 °C for 2 min [98 °C for 10 sec, 59 °C for 10 sec, 72 °C for 1 min] × 35 cycles, 72 °C for 5 min, and then held at 4 °C until further analysis. PCR products (20-40 µL) were ran on a 2% agarose gel. The iBright CL1500 imaging system (Invitrogen,Waltham, MA, USA) was used to visualize amplicon bands. Bands containing gene of interest was extracted and purified from the agarose gel using the Monarch® DNA Gel Extraction Kit (New England Bioloabs, #T1020S, Ipswich, MA, USA). The mutation was confirmed by Sanger sequencing using the Genewiz from Azenta life sciences (South Plainfield, NJ, USA) platform to confirm sequence accuracy.

For semi-quantitative data, each band was quantified using the 'Analyze > Gel' function on Fiji software. Each band of *USH2A* exon 13 skip was normalized to *USH2A* full-length level. Each experiment was carried out in triplicate.

Human pluripotent stem cell lines and culture

a. *Cell lines.* Human IEOs and ROs were derived from SOX2-GFP (parental line WTC-11) hiPSC line that has been purchased from Allen Institute for Cell Science and the Coriell Institute. This cell line was used in previous publications to generate IEOs successfully (figure 4A) (Steinhart et al., 2023; Valk et al., 2023). The cell line was tested negative for mycoplasma contamination and genetic abnormalities (karyotyping) prior to experimentation. Detailed information of the cell line validation and testing is available at https://www.allencell.org/cell-catalog.htm. *USH2A* mutant cell line (C20) generation has been outsourced to Synthego Corporation (now EditCo). Briefly, a gene variant in exon 13 (*c.2299delG*) of *USH2A* (Transcript ID: ENST00000307340.8) was introduced to SOX2-GFP (control) cell line using specially designed CRISPR/Cas9 gRNA (sequence: AAUUCUGCAAUCCUCACUCU) and a ssODN donor sequence (TGCCAGTGTAACCTCCATGGC-TCAGTGAACAAATTCTGCAATCCTCATTCTGGGCAGTGTAGTGCAAAAAAGAAGCCAAAGGACT TCAGTGTGACACCTGCAGAGAAAACTTTTATGGGTTA; see figure S6A-B). All edited clones were tested for mycoplasma (InvivoGen, MycoStrip-Mycoplasma Detection Kit, #rep-mysnc-50, San Diego, CA, USA), normal karyotype (figure S6C, Thermo Fisher Scientific, KaryoStat+ Genetic Stability Assay Service, #A52849, Waltham, MA, USA), and pluripotency (figure S6D), prior to differentiation.

b. *Cell culture and maintenance.* Medium needs to be pre-warmed at RT for 15-20 min before use. *Thawing:* The cryopreserved hiPSC lines were thawed in Essential 8™ Flex medium (hereafter, E8; Thermo Fisher Scientific, Gibco™, #A2858501, Waltham, MA, USA) containing 100 μg/mL Normocin® (antibiotics, InvivoGen, #ant-nr-1, San Diego, CA, USA) and 10 μM Stemolecule™ Y27632 (hereafter, Y; Reprocell, Stemgent, #04-0012-02, Beltsville, MD, USA), a Rho-associated kinase inhibitor that prevents cells undergoing apoptosis and increase cell viability. The thawed cells

were cultured on a vitronectin-coated (0.5 μg/cm^2, Thermo Fisher Scientific, Gibco™, #A14700, Waltham, MA, USA) 6-well culture plate. After 24 hrs of thawing, the Y containing spent medium was replenished with fresh E8 medium containing 100 μg/mL Normocin®, without Y. *Maintenance:* The spent medium was replenished every other day or daily, depending on hiPSC confluency, with 2-3 mL of fresh E8 medium containing 100 μg/mL Normocin® per well. The hiPSCs were passaged when they have reached at 80% of confluency, typically 4-5 days post thawing or passaging. *Passaging:* Spent medium was aspirated out and the hiPSCs were rinsed twice with 1X DPBS. Using StemPro™ Accutase™ Cell Dissociation Reagent (hereafter, Accutase; Thermo Fisher Scientific, Gibco™, #A1110501, Waltham, MA, USA), the hiPSCs were passaged in small clusters (5-6 cells per cluster) in E8 medium containing 100 μg/mL Normocin® and 10 μM Y. The Y containing medium was replenished and the cells were further maintained as described in thawing and maintenance.

c. *Human IEO differentiation.* To initiate IEO differentiation, the hiPSC colonies in maintenance culture were detached and dissociated into single cells using Accutase. The dissociate single cells were resuspended in E8 medium containing 100 μg/mL Normocin® and 20 μM Y. The number of live cells in the cell suspension was determined, and the cells were seeded at a density of 3,500 cells in a 100 μL per well in a Nunclon™ Sphera™ 96-well Nunclon Sphera-Treated U-Shaped-Bottom Microplate (hereafter, 96-well plate; Thermo Fisher Scientific, #174927, Waltham, MA, USA). After the cells were seeded, the 96-well plate was centrifuged at 110 g for 6 min, followed by incubation in a 37 ºC incubator with 5% CO_2. This cell pre-aggregation timepoint was designated as *day -2*. Twenty-four hours after pre-aggregation (*day -1*), 100 μL of fresh E8 medium containing 100 μg/mL Normocin®, without Y, was added to each well using a multi-channel pipette to dilute Y and promote normal cell proliferation. After another 24 hours (*day 0*), differentiation was initiated. Each aggregate in the 96-well plate was collected and individually transferred into a new 96-well plate, with 100 μL per well of *day 0 differentiation medium*. The medium consisted of ice-cold Essential 6™ medium (hereafter, E6; Thermo Fisher Scientific, Gibco™, #A1516401, Waltham, MA, USA) supplemented with 2%

Matrigel™ Growth Factor Reduced Basement Membrane Matrix (hereafter, Matrigel; Corning, #356231, Corning, NY, USA), 10 μM Stemolecule™ SB431542 (a TGFβ inhibitor; Reprocell, Stemgent, #04-0010-05, Beltsville, MD, USA), 4 ng/mL Human FGF-basic (154aa) Recombinant Protein (fibroblast growth factor, hereafter, bFGF; Thermo Fisher Scientific, PeproTech, #100-18B-50UG, Waltham, MA, USA), 1.25 ng/mL Human BMP-4 Recombinant Protein (bone morphogenetic protein 4, hereafter, BMP4; Thermo Fisher Scientific, PeproTech, #120-05-5UG, Waltham, MA, USA), and 100 μg/mL Normocin®. This procedure can be performed by transferring all aggregates to a 100 mm Petri-dish using a multi-channel pipette with wide-orifice p200 tips. The aggregates are then collected in a 2 mL round-bottom tube using a wide-orifice p1000 tip, washed three times with E6 medium, resuspended in ice-cold *day 0 differentiation medium*, and transferred into a 100 mm Petri-dish containing ice-cold *day 0 differentiation medium*, kept on ice. Using a wide-orifice p200 tip on a pipette, transfer individual aggregate into each well of a new 96-well plate. Then, incubate the aggregate containing plate in a 37 ºC incubator with 5% CO_2 for three days. On day 3 of differentiation, the aggregates were treated with Stemolecule™ LDN-193189 (a BMP inhibitor, hereafter, LDN; Reprocell, Stemgent, #04-0074-02, Beltsville, MD, USA) and bFGF at final concentrations of 200 nM and 50 ng/mL, respectively, in E6 medium containing 100 μg/mL Normocin®. To achieve these final concentrations, 25 μL of E6 medium containing LDN and bFGF at 5x concentrations (1 μM and 250 ng/mL, respectively) was added per well, resulting in a total volume of 125 μL per well. On day 6, 75 μL of fresh E6 medium containing 100 μg/mL Normocin® was added to each well, resulting in a final volume of 200 μL per well. The plate was gently tapped to mix the medium and incubated in a 37 ºC incubator with 5% CO_2 for two days. On day 8 of differentiation, otic induction was initiated. Using a multi-channel pipette, 100 μL of spent medium was removed from each well and replaced with 100 μL of fresh E6 medium containing 100 μg/mL Normocin® and 6 μM Stemolecule™ CHIR99021 (hereafter, CHIR; Reprocell, Stemgent, #04-0004-02, Beltsville, MD, USA) at 2x concentration. This results in a final volume of 200 μL per well, with CHIR at a final concentration of 3 μM (1x). Otic induction continued on day 10 by replenishing half of the medium (100 μL) in each well with 100 μL

of freshly prepared E6 medium containing 100 μg/mL Normocin® and 3 μM CHIR, followed by a 2-day incubation at 37 ºC in a 5% CO_2 incubator. On day 12, the aggregates were transitioned to self-assembly stage in a floating culture. All aggregates in 96-well U-bottom plates are individually picked and collected in a 100 mm petri-dish using a wide-orifice p1000 tip. All aggregates were centered by gentle swirl of the dish and collected and transferred to a 2 mL round-bottom tube using a wide-orifice p1000 tip. The aggregates were carefully rinsed for three times in 1 mL of Advanced DMEM/F12 medium (Thermo Fisher Scientific, Gibco™, #12634010, Waltham, MA, USA) per rinse and transferred into organoid maturation medium (OMM) containing 1% Matrigel and 3 μM CHIR (hereafter, OMM1%M-CH) prepared and placed on ice. OMM is composed of Advanced DMEM/F12 and Neurobasal™ (Thermo Fisher Scientific, Gibco™, #21103049, Waltham, MA, USA) media at 1:1 ratio, supplemented with 0.5x N2 Supplement (100x; Thermo Fisher Scientific, Gibco™, #17502048, Waltham, MA, USA), 0.5x B-27™ Supplement minus vitamin A (50x; Thermo Fisher Scientific, Gibco™, #12587010, Waltham, MA, USA), 1x GlutaMAX™ (Thermo Fisher Scientific, Gibco™, #35050061, Waltham, MA, USA), 0.1 mM 2-Mercaptoethanol (Thermo Fisher Scientific, Gibco™, #21985023, Waltham, MA, USA), and 100 μg/mL Normocin®. Using a wide-orifice p1000 tip, individual organoid was transferred into each well on Nunclon™ Sphera™ 24-well low-attachment plates (Thermo Fisher Scientific, #174930, Waltham, MA, USA) in 500 μL of OMM1%M-CH per well, followed by 72 hrs incubation in a 37 ºC incubator with 5% CO_2. Starting from day 12, the plates were incubated on an orbital shaker placed in an incubator. On day 15 , half of the spent medium (250 μL) was replenished with 250 μL of freshly prepared OMM 1% M-CH to continue otic vesicle induction. Gently swirled the plates to mix medium and cultured in the incubator for 72 hrs. On day 18 of differentiation, half of the medium was replaced with fresh OMM to dilute Matrigel and CHIR while providing nutrients. Starting from day 21 of differentiation, a full-medium change was performed once a week by carefully aspirating out all medium from each well and adding 500 μL of freshly prepared OMM. Within this one-week period, half-medium change was performed every three days until day 45. After day 45, the half-medium change was performed every other day, with the necessity of

increasing the medium volume to 1-1.5 mL per well as the aggregate size grew larger and medium color turns yellow more quickly.

d. Human RO differentiation.

i. *Protocol 1*: For RO differentiation, the hiPSCs were maintained in mTeSR™ Plus medium (STEMCELL Technologies, #100-0276, Vancouver, BC, Canada). When the iPSC colonies reached 80% confluency, the cells were detached and dissociated into single cells using Accutase as described in the IEO differentiation section. The cells were collected, centrifuged, and resuspended in mTeSR™ Plus containing 20 μM Y (hereafter, mTeSR™ Plus + Y). After determining live cell numbers in the single cell suspension, the cells were seeded at 3,000 cells per 100 μL of mTeSR™ Plus +Y per well in a 96-well plate and centrifuged prior to incubation in a 37 ºC incubator with 5% CO_2 for 24 hrs. This step was referred to as day -1. On day 0, 100 μL of a medium mixture of mTeSR™ Plus and neural induction medium (NIM), mixed at a 1:1 ratio, was added to each well, resulting in a final volume of 200 μL per well and a final media ratio of 3:1 (mTeSR™ Plus:NIM). The NIM is based on DMEM/F12, HEPES medium (Thermo Fisher Scientific, Gibco™, #11330032, Waltham, MA, USA) supplemented with 1x N2, 1x MEM Non-Essential Amino Acids (NEAA, 100x; Thermo Fisher Scientific, Gibco™, #11140050, Waltham, MA, USA), 1x penicillin-streptomycin (10,000 U/mL; Sigma-Aldrich, #P4333-100ML, St. Louis, MO, USA), and 2 μg/mL Heparin (Sigma-Aldrich, #H3149-50KU, St. Louis, MO, USA). From day 0 to day 2 of differentiation, the proportion of mTeSR™ Plus is gradually decreased, transitioning fully to NIM by day 3; i.e., the ratio of mTeSR™ Plus:NIM changes from 3:1 (day 0), to 1:1 (day 1), and to 1:3 (day 2). On day 1, all the aggregates were collected, rinsed, and transferred to 100 μL of 1:1 mTeSR™ Plus:NIM medium per well in a 96-well plate. On day 2, 100 μL of NIM was added to each well, resulting in a total volume of 200 μL per well and a final media ratio of 1:3 (mTeSR™ Plus:NIM). On day 3, all aggregates

from the 96-well plate were collected into a 100 mm Petri-dish, transferred to a 2 mL round-bottom tube using a wide-orifice p1000 tip, and carefully rinsed twice with 1 mL of NIM per wash. After the last wash, 1 mL of NIM was added to the tube containing the aggregates, which were then transferred to new 100 mm Petri-dishes containing 10 mL of NIM, with 30-45 aggregates per dish. The dishes were gently swirled and shaken to evenly distribute the aggregates and prevent aggregate-to-aggregate merging. The dishes were incubated in a 37ºC incubator with 5% CO_2 for three days. On day 6 of differentiation, the aggregates were collected, rinsed once with NIM, and resuspended in NIM containing 1.5 nM BMP4 (hereafter, NIM+B). To a non-tissue culture-treated (or low-attachment) 6-well plate containing 2 mL of NIM+B, 10-15 aggregates were added per well in 500 µL NIM+B, resulting in a final volume of 2.5 mL NIM+B per well. The plate was gently swirled and shaken to evenly distribute the aggregates, then incubated in a 37ºC incubator with 5% CO_2 for two days. On day 8, 500 µL of fetal bovine serum (FBS; Thermo Fisher Scientific, Gibco™, #16140071, Waltham, MA, USA) was added to a tissue culture-treated 6-well plate, ensuring the surface of each well was evenly coated. Then, aggregates cultured in NIM+B were transferred to the FBS containing wells along with 2 mL of the spent NIM+B. The aggregates were evenly distributed within each well and incubated in a 37 ºC incubator with 5% CO_2 for 24 hrs. On days 9 and 12, half of the spent medium (1 mL) was removed and replaced with 1 mL of fresh NIM without FBS. On day 15, the entire medium was aspirated, and 2 mL of fresh NIM was added. On day 16, adhering aggregates on the plate surface were detached using the tip of a p200 pipette tip and transferred to a 15 mL conical tube. The aggregates were rinsed three times and resuspended in retinal differentiation medium (RDM) containing 1% FBS. RDM is composed of DMEM/F12 and DMEM-high glucose (Thermo Fisher Scientific, Gibco™, #12430054, Waltham, MA, USA) media mixed at a 1:1 ratio, supplemented with 1x B-27™ Supplement with vitamin A, serum free (50x; Thermo Fisher Scientific, Gibco™, #17504044, Waltham, MA, USA), 1x MEM NEAA, and 1x penicillin-streptomycin. Then, the aggregates were transferred to a

100 mm Petri-dish containing 10 mL of RDM supplemented with 1% FBS. On days 18 and 20, the spent medium was carefully replenished with 10 mL of RDM supplemented with 3% and 5% FBS, respectively. On day 22 of differentiation, the spent medium was replenished with 2 mL of RDM containing 10% FBS and 1x GlutaMAX™. From day 25 to day 50 of differentiation, the medium was replenished with retinal maturation medium (RMM) every 2-3 days. RMM is based on RDM, supplemented with 10% FBS, 1x GlutaMAX™, and 100 μM Taurine (Sigma-Aldrich, #T0625-10G, St. Louis, MO, USA). Note that Taurine should be freshly added at each medium change. On day 50, the medium was switched to advanced retinal maturation medium (ARMM), which based on RMM and supplemented with 1 μM All-trans-Retinoic Acid (RA; Thermo Fisher Scientific, Acros Organics™, #207341000, Waltham, MA, USA) and 20 ng/mL brain-derived neurotrophic factor (BDNF; Thermo Fisher Scientific, PeproTech, #450-02-50UG, Waltham, MA, USA). From day 50 to day 90, the spent medium was replenished every 2-3 days with fresh ARMM. From day 90 and onward, the spent medium was replenished every 2-3 days with fresh ARMM without RA.

ii. *Protocol 2*: This protocol was adapted from Capowski et al. (2019). Detailed steps are briefly described below. On day 0, hiPSC colonies in maintenance culture at approximately 80% confluency were detached from the plate into small cell pellets (5–20 cells per pellet) using 0.5 mM EDTA (Thermo Fisher Scientific, Invitrogen™, #15575020, Waltham, MA, USA). The cell pellets were collected in E8 medium supplemented with 20 mM Y-27632 (hereafter, E8 + Y) and then transferred into a T75 flask (Thermo Fisher Scientific, #156800, Waltham, MA, USA) pre-treated with Anti-Adherence Rinsing Solution (Stemcell Technologies, #07010, Waltham, MA, USA), or into other ultra-low attachment T75 flasks without additional anti-adherence treatment. The flasks were incubated statically and horizontally in a 37□°C incubator with 5% CO_2 overnight. During this period, cell pellets self-assembled into embryoid bodies (EBs). From day 1 to day 4 of differentiation, the

proportion of E8 was gradually decreased, transitioning fully to neural induction medium (NIM) by day 4. Specifically, the ratio of E8:NIM was adjusted as follows: 2:1 (day 1), 1:1 (day 2), and 1:2 (day 3). NIM was based on DMEM/F12 (Thermo Fisher Scientific, Gibco™, #11330032, Waltham, MA, USA), supplemented with 1% N2 Supplement (Thermo Fisher Scientific, Gibco™, #17502048, Waltham, MA, USA), 1x MEM Non-Essential Amino Acids (100x; Thermo Fisher Scientific, Gibco™, #11140076, Waltham, MA, USA), 1x GlutaMAX (100x; Thermo Fisher Scientific, Gibco™, #35050079, Waltham, MA, USA), 2 mg/mL Heparin (Sigma-Aldrich, #H3149-50KU, St. Louis, MO, USA), and Sodium Pyruvate (Thermo Fisher Scientific, Gibco™, #11360070, Waltham, MA, USA). On day 6, 10–25 ng/mL of human bone morphogenetic protein 4 (BMP4, PeproTech, #120-05-100UG) was added to fresh NIM. The concentration of BMP4 varied by cell line and needed to be titrated for each new line. On day 7, EBs were collected and distributed into 6-well plates pre-coated with 9.5 mg/mL Matrigel. The plates were gently swirled and shaken to evenly distribute the EBs, then incubated in a 37□°C incubator with 5% CO_2 for two days. On days 9, 12, and 15, half of the media was replaced with fresh NIM to progressively decrease the BMP4 concentration. On day 16, the medium was replaced with retinal differentiation medium containing retinoic acid (hereafter, RDM), composed of a 3:1 mixture of High Glucose DMEM (Thermo Fisher Scientific, Gibco™, #11965092, Waltham, MA, USA) and Ham's F-12 Nutrient Mix (Thermo Fisher Scientific, Gibco™, #11765054, Waltham, MA, USA) (hereafter, HG-DMEM/F12 3:1), supplemented with 1x penicillin-streptomycin (Sigma-Aldrich, #A5955-20M, St. Louis, MO, USA) and 2% B27 Supplement with retinoic acid (50x; Thermo Fisher Scientific, Gibco™, #17505044). From day 16 to day 25, the 6-well plates were replenished with fresh RDM. Between days 25–30, 3D optic vesicles (OVs) became apparent and were manually lifted using a stab knife (Ambler Surgical, #7536, Exton, PA, USA). The floating OVs were collected and transferred into ultra-low attachment T25 flasks (Thermo Fisher Scientific, Gibco™, #174951) containing fresh 3D medium. This medium was composed of HG-DMEM/F12

3:1, 2% B27 Supplement, 5% FBS, 1x MEM-NEAA, 1x GlutaMAX, 100 µM Taurine (Sigma-Aldrich, #T0625-10G), 1x penicillin-streptomycin, and chemically defined lipid supplement (Thermo Fisher Scientific, Gibco™, #11905031). From this point forward, the medium was replenished with fresh 3D medium every 2-3 days.

Immunohistochemistry

*Sample preparation: Fixation***.** IEOs and ROs that reached the timepoints of interest were collected in 2 mL round-bottom tubes using a wide-orifice p1000 tip cut to an appropriate diameter that kept organoids intact. Collected organoids were rinsed twice with 1 mL of 1x Phosphate Buffered Saline (PBS, Thermo Fisher Scientific, Gibco™, #10010023, Waltham, MA, USA) per rinse and fixed in 4% paraformaldehyde (PFA, Electron microscopy sciences, #15710, Hatfield, PA, USA) overnight at 4 ºC on a rocking shaker. Fixed organoids were washed three times with 1 mL of 1X PBS, 10 min per wash, on a rocking shaker at RT. After the final wash, the solution was replenished with fresh 1x PBS, and the samples were processed for next steps or stored at 4 ºC.

Cryo-embedding and preservation. The fixed and washed samples were introduced to 15% sucrose and incubated at RT on a rocking shaker for 30 min or until all aggregates sank to the bottom of the tubes. Then, the solution was switched to 30% sucrose and incubated on a rocking shaker at RT for ~1 hr or until all aggregates sank to the bottom. Once the aggregates were adapted to sucrose, using a wide-orifice tip or a perforated spoon, we transfered them to a Tissue-Tek® cryo-mold (Sakura Finetek, #4565 or #4566, Torrance, CA, USA). Under a stereomicroscope, we carefully removed residual sucrose from the mold using a blunt-end needle and 1 mL syringe and oriented the organoids to a desired orientation. Then, gently added Tissue-Tek® O.C.T. Compound (hereafter, OCT freezing medium; SAKURA, #4583, Torrance, CA, USA) to the cry-mold, ensuring the organoids remain in the same position and orientation. In case of organoids floating in the OCT freezing medium or change in their orientation, we used a blunt-end needle to gently reposition them at the bottom of the mold in the correct orientation, performed slow and cautiously as the OCT freezing medium was viscous. Next, we snap-froze the mold on dry-ice until the OCT freezing medium turned opaque. The frozen cryo-mold was then stored in a sealed container at -80 ºC or used for cry-sectioning after freezing at least 1 hr longer in -80 ºC**.** *Cryo-sectioning*: We

pre-adapted the temperature of the cryo-mold to match that inside a cryostat, typically -23 ºC, by leaving the block inside the cryostat for at least 20 min. Sections were cut at 12 μm thickness onto slide glasses, with an average of three sections per slide. The slide glasses with sections were labeled, placed in a box, and desiccated in a desiccator for one hour with the box lid open. After desiccation, the box lid was closed, and the slides were stored at -80 ºC until use.

Immunostaining: The slides that were stored in -80 ºC were thawed and dried at RT, drew outline surrounding the section area using a PAP pen (Electron Microscopy Sciences, #71310, Hatfield, PA, USA), and dried PAP pen for 1-2 min. Hydrate the sections by placing the slides in a Coplin jar containing 1x PBS and incubating for 10 min. Then, take out the slides, remove excess solution outside of PAP pen-outline, and place on a humidified staining chamber containing MilliQ water. Carefully add 150 μL of blocking solution per slide in a drop-wise manner. The blocking solution is based on 1x PBS-T (0.1% Triton X-100) supplemented with 10% Normal Goat Serum Blocking Solution (hereafter, NGS; Vector Laboratories, #S-1000-20, Newark, CA, USA) or Normal Horse Serum Blocking Solution (hereafter, NHS; Vector Laboratories, #S-2000-20, Newark, CA, USA), depending on the hosts of antibodies. Close the lid of the chamber and incubate at RT for 1 hr. After blocking, remove the solution by gently tilting the slide glass at an angle from one corner and place it back in the chamber. Gently add primary antibody mixture prepared in 3% NGS or NHS in 1x PBS-T, in a drop-wise manner. A 100 μL volume is sufficient to cover the sections on one slide. Antibodies information is listed in *Table S11*. Incubate the primary antibodies for 1 hr and 15 min at RT with the chamber lid closed. Then, tilt the slide at an angle from one corner to remove primary antibodies-mixture and place it in a Coplin jar containing 1x PBS for washing. Wash in 1x PBS for three times, 10 min per wash, on an orbital shaker at RT. After the last wash, remove residual PBS outside the PAP pen-outline, and place the slides in the chamber. Gently add 150 μL of the appropriate secondary antibody mixture, including DAPI or Hoechst, prepared in 3% NGS or NHS in 1x PBS-T, to each slide in a drop-wise manner. After 1 hr incubation with the secondary antibodies, remove the solution and wash the slides three times with 1x PBS in a Coplin jar, allowing 10 min per wash. In the meantime, discard the MilliQ water from the humidified chamber and dry it. After the final wash, remove excess PBS on the slide glass and place the slide in the dried chamber. Be cautious not to let the sample sections dry out. Then, very gently, in a

drop-wise manner and avoiding bubble formation, add 3 drops of ProLong™ Gold Antifade Mountant (Thermo Fisher Scientific, Invitrogen™, #P36930 or #P36931, Waltham, MA, USA) to the sections. Carefully cover the sections with a coverslip. Place the chamber containing the slides in dark with the lid off for overnight, allowing the mounting solution to dry and stabilize. The next day, seal any potential gaps between the slide glass and coverslip using transparent nail polish. Once the nail polish is dry, the slides are ready for imaging. Microscopy was performed using Nikon A1R confocal microscope.

Live organoid vibratome sectioning

Sample preparation: A 2% Low Melting Point Agarose (LMPA) solution was prepared by dissolving 2 g of UltraPure LMPA powder (Invitrogen) in 100 mL of double-distilled water in a Schott media bottle using a microwave, heating in 10-15 sec pulses with intermittent swirling. A magnetic stir bar was added to the bottle and the dissolved LMPA was then placed on a hot plate set 41 ºC with stirring at 75 rpm and allowed to cool to 41 ºC. Organoids were collected in a 2 mL U-bottom tube, rinsed three times with 1mL of 1X DPBS, and transferred to a cryomold using a cut wide-orifice p1000 tip. Excess DPBS was removed from the mold using a syringe fitted with a blunt-end needle. The cooled LMPA was added to the mold, and the organoids were arranged in the desired orientation and allowed to settle at the bottom of the mold. If necessary, a blunt-end needle or p20 tip was used for positioning. The mold was then placed on ice on a flat surface to allow the agarose to polymerize.

Vibratome sectioning. The LPMA-organoid block was carefully dislodged from the mold, and excess moisture was gently blotted with a Kimwipe. The block was flipped so that the organoids faced upward and was placed on the mold holder of a metal buffer tray, secured with superglue. The buffer tray was then inserted into the vibratome (Leica, VT1000S), and ice-cold, sterile 1X DPBS was added to cover the top surface of the LMPA-organoid block, with the outer tray filled with ice. The LMPA-organoid block was sectioned with a speed 4 and frequency of 4 either at 200 µm thickness for multiple slices to be produced, or at 500 µm thickness to cut the organoid approximately in half. Each slice was collected as it floated off using a flat metal spoon (precision instruments) and transferred to a non-tissue-treated 6-well culture plate filled with ice-cold 1X DPBS on ice. In a

biosafety cabinet, slices were transferred to pre-warmed OMM in a 100 mm petri-dish to recover. Using sterile forceps, organoids were carefully dislodged from LMPA. Isolated organoid slices were then transferred to a glass-bottom 24-well plate for AAV transduction and imaging.

AAV/ASO transduction in organoids

To evaluate virus titration and transduction efficiency of selected capsids, human IEOs derived from control (IEO^{SOX2}) and *USH2A* mutant (IEO^{C20}) iPSC lines, at differentiation days (D) 46, 52, 91, 118, and 125, were vibratome-sectioned into 2-6 slices per organoid, depending on their age and size, to optimize hair cell exposure for transduction, followed by a day of recovery. ROs derived from the same cell lines (RO^{SOX2} and RO^{C20}), at differentiation days D90, 112, 148, and 168, were used without vibratome sectioning, as photoreceptors are developed in the outer layer of organoids, making them readily accessible for transduction. Both sliced IEOs and intact ROs were transduced with AAV9-PHP.B-CMV-Skipper-mKate, AAV9-PHP.B-CMV-mKate-empty, AAV2-7m8-CMV-Skipper-mKate, AAV2-7m8-CMV-GFP-empty, or left untransduced as controls. An AAV titer of 5 x

viral genomes (vg) in 500 µL of OMM per well in a 24-well plate was used for all conditions. Following transduction, organoids were cultured at 37 ºC in a 5.0% CO_2 incubator for 3 days (72 hrs). Three days post-transduction, the virus-containing medium was replaced with fresh OMM, and organoids were subsequently maintained for an additional 11-13 days (14-16 days post-initial AAV transduction) before collection. On differentiation days 67, 73, 79, 87 106, 118, and 141 for IEOs and days 105, 128, 162, and 183 for ROs, the organoids were harvested for RNA extraction, processed for confocal live-cell imaging, or fixed for immunostaining. AAV9-PHP.B and AAV2-7m8 capsids were tested using the same viral concentration and the incubation time.

Statistical analyses

Data were analyzed with GraphPad version 9 software (Boston, MA, USA) as mean ± standard deviation (S.D.).

DATA AVAILABLITY STATEMENT

All data supporting the findings of this study are available within the paper and its supplemental information.

ACKNOWLEDGEMENTS

Gene-therapy research in the Holt/Geleoc lab is supported by the Jeffrey and Kimberly Barber Fund for Gene Therapy Research, the Usher Syndrome Society and by the IDDRC (grant 1U54HD090255) and the Neurodevelopmental Behavioral and Viral Cores at Boston Children's Hospital. Work on this project was also supported BioMarin Pharmaceutical. The authors would like to thank Elizabeth Del Greco, Vincent Leonard, Leonor Miranda-Newquist, Darlene Chen, Terri Christianson, Hassib Akeefe and Pooja Agarwal for design, generation and characterization of viral vectors. The authors would also like to thank Jason Meyer, Jade Harkin, David Gamm, and Marcela Garita-Hernandez for technical assistance with generation of retinal organoids and Peter Colosi for constructive review of the project and data.

AUTHOR CONTRIBUTIONS

SAM: Conceptualization, Investigation, Analysis, Visualization, Writing – original draft; JL: Investigation, Supervision, Visualization, Writing – review & editing; JZ: Methodology, Investigation, Writing – review & editing; JJ: Investigation, Visualization, Writing – review & editing; CN-L: Investigation, Visualization, Writing – review & editing; CTM: Investigation, Visualization, Writing – review & editing; CRVM: Investigation, Formal analysis, Visualization, Writing – review & editing; SO: Investigation, Formal analysis, Writing – review & editing; MGC: Validation, Writing – review & editing; MAM.: Formal analysis, Writing – review & editing; KF: Formal analysis, Writing – review & editing; SL: Project Administration, Conceptualization, Methodology, Writing – review & editing; CJ: Investigation, Writing – review & editing; SRK: Resources, Writing – review & editing; SR: Resources, Writing – review & editing; JI: Supervision, Project administration, Funding acquisition; Writing – review & editing; KRK: Methodology, Supervision, Writing – review & editing; JRH: Conceptualization, Funding acquisition, Project administration, Supervision, Writing – review & editing; GSGG: Conceptualization, Project administration, Supervision, Writing – review & editing;

DECLARTATION OF INTERESTS

Shinong Long, Chris Jacobs, Peter Colosi, Sripriya Ravindra Kumar, Silvia Ramirez and Justin Ichida are employees of BioMarin Pharmaceutical. Jeffrey R. Holt holds a patent on the use of AAV9-PHP.B for gene therapy in the inner ear. The authors declare no other conflicts of interest.

KEYWORDS

Usher Syndrome, deaf-blindness, Usherin, USH2A, Antisense Oligonucleotide, ASO, adeno-associated virus, AAV, Inner ear organoid, retinal organoid

REFERENCES

1. Afanasyeva, T.A.V., Corral-Serrano, J.C., Garanto, A., Roepman, R., Cheetham, M.E., and Collin, R.W.J. (2021). A look into retinal organoids: methods, analytical techniques, and applications. Cell Mol Life Sci 78, 6505-6532. 10.1007/s00018-021-03917-4.

2. Aparisi, M.J., Aller, E., Fuster-Garcia, C., Garcia-Garcia, G., Rodrigo, R., Vazquez-Manrique, R.P., Blanco-Kelly, F., Ayuso, C., Roux, A.F., Jaijo, T., and Millan, J.M. (2014). Targeted next generation sequencing for molecular diagnosis of Usher syndrome. Orphanet J Rare Dis 9, 168. 10.1186/s13023-014-0168-7.

3. Besnard, T., Vache, C., Baux, D., Larrieu, L., Abadie, C., Blanchet, C., Odent, S., Blanchet, P., Calvas, P., Hamel, C., Dollfus, H., et al. (2012). Non-USH2A mutations in USH2 patients. Hum Mutat 33, 504-510. 10.1002/humu.22004.

4. Bonnet, C., Grati, M., Marlin, S., Levilliers, J., Hardelin, J.P., Parodi, M., Niasme-Grare, M., Zelenika, D., Delepine, M., Feldmann, D., Jonard, L., et al. (2011). Complete exon sequencing of all known Usher syndrome genes greatly improves molecular diagnosis. Orphanet J Rare Dis 6, 21. 10.1186/1750-1172-6-21.

5. Capowski, E.E., Samimi, K., Mayerl, S.J., Phillips, M.J., Pinilla, I., Howden, S.E., Saha, J., Jansen, A.D., Edwards, K.L., Jager, L.D., Barlow, K., et al. (2019). Reproducibility and staging of 3D human retinal organoids across multiple pluripotent stem cell lines. Development 146. 10.1242/dev.171686.

6. Carss, K.J., Arno, G., Erwood, M., Stephens, J., Sanchis-Juan, A., Hull, S., Megy, K., Grozeva, D., Dewhurst, E., Malka, S., Plagnol, V., et al. (2017). Comprehensive Rare Variant Analysis via Whole-Genome Sequencing to Determine the Molecular Pathology of Inherited Retinal Disease. Am J Hum Genet 100, 75-90. 10.1016/j.ajhg.2016.12.003.

7. Crane, R., Tebbe, L., Mwoyosvi, M.L., Al-Ubaidi, M.R., and Naash, M.I. (2023). Expression of the human usherin c.2299delG mutation leads to early-onset auditory loss and stereocilia disorganization. Commun Biol 6, 933. 10.1038/s42003-023-05296-x.

8. Dalkara, D., Byrne, L.C., Klimczak, R.R., Visel, M., Yin, L., Merigan, W.H., Flannery, J.G., and Schaffer, D.V. (2013). In vivo-directed evolution of a new adeno-associated virus for therapeutic outer retinal gene delivery from the vitreous. Sci Transl Med 5, 189ra176. 10.1126/scitranslmed.3005708.

9. Dona, M., Slijkerman, R., Lerner, K., Broekman, S., Wegner, J., Howat, T., Peters, T., Hetterschijt, L., Boon, N., de Vrieze, E., Sorusch, N., et al. (2018). Usherin defects lead to early-onset retinal dysfunction in zebrafish. Exp Eye Res 173, 148-159. 10.1016/j.exer.2018.05.015.

10. Dreyer, B., Tranebjaerg, L., Rosenberg, T., Weston, M.D., Kimberling, W.J., and Nilssen, O. (2000). Identification of novel USH2A mutations: implications for the structure of USH2A protein. Eur J Hum Genet 8, 500-506. 10.1038/sj.ejhg.5200491.

11. Dulla, K., Slijkerman, R., van Diepen, H.C., Albert, S., Dona, M., Beumer, W., Turunen, J.J., Chan, H.L., Schulkens, I.A., Vorthoren, L., den Besten, C., et al. (2021). Antisense oligonucleotide-based treatment of retinitis pigmentosa caused by USH2A exon 13 mutations. Mol Ther 29, 2441-2455. 10.1016/j.ymthe.2021.04.024.

12. Dulon, D., Papal, S., Patni, P., Cortese, M., Vincent, P.F., Tertrais, M., Emptoz, A., Tlili, A., Bouleau, Y., Michel, V., Delmaghani, S., et al. (2018). Clarin-1 gene transfer rescues auditory synaptopathy in model of Usher syndrome. J Clin Invest 128, 3382-3401. 10.1172/JCI94351.

13. Gadgil, A., and Raczynska, K.D. (2021). U7 snRNA: A tool for gene therapy. J Gene Med 23, e3321. 10.1002/jgm.3321.

14. Garita-Hernandez, M., Routet, F., Guibbal, L., Khabou, H., Toualbi, L., Riancho, L., Reichman, S., Duebel, J., Sahel, J.A., Goureau, O., and Dalkara, D. (2020). AAV-Mediated Gene Delivery to 3D Retinal Organoids Derived from Human Induced Pluripotent Stem Cells. Int J Mol Sci 21. 10.3390/ijms21030994.

15. Garita-Hernandez, M., Routet, F., Guibbal, L., Khabou, H., Toualbi, L., Riancho, L., Reichman, S., Duebel, J., Sahel, J.A., Goureau, O., and Dalkara, D. (2020). AAV-Mediated Gene Delivery to 3D Retinal Organoids Derived from Human Induced Pluripotent Stem Cells. Int J Mol Sci 21. 10.3390/ijms21030994.

16. Goyenvalle, A., Vulin, A., Fougerousse, F., Leturcq, F., Kaplan, J.C., Garcia, L., and Danos, O. (2004). Rescue of dystrophic muscle through U7 snRNA-mediated exon skipping. Science 306, 1796-1799. 10.1126/science.1104297.

17. Harkin, J., Pena, K.H., Gomes, C., Hernandez, M., Lavekar, S.S., So, K., Lentsch, K., Feder, E.M., Morrow, S., Huang, K.C., Tutrow, K.D., et al. (2024). A highly reproducible and efficient method for retinal organoid differentiation from human pluripotent stem cells. Proc Natl Acad Sci U S A 121, e2317285121. 10.1073/pnas.2317285121.

18. Isgrig, K., McDougald, D.S., Zhu, J., Wang, H.J., Bennett, J., and Chien, W.W. (2019). AAV2.7m8 is a powerful viral vector for inner ear gene therapy. Nat Commun 10, 427. 10.1038/s41467-018-08243-1.

19. Isgrig, K., Shteamer, J.W., Belyantseva, I.A., Drummond, M.C., Fitzgerald, T.S., Vijayakumar, S., Jones, S.M., Griffith, A.J., Friedman, T.B., Cunningham, L.L., and Chien, W.W. (2017). Gene Therapy Restores Balance and Auditory Functions in a Mouse Model of Usher Syndrome. Mol Ther 25, 780-791. 10.1016/j.ymthe.2017.01.007.

20. Ivanchenko, M.V., Hathaway, D.M., Klein, A.J., Pan, B., Strelkova, O., De-la-Torre, P., Wu, X., Peters, C.W., Mulhall, E.M., Booth, K.T., Goldstein, C., et al. (2023). Mini-PCDH15 gene therapy rescues hearing in a mouse model of Usher syndrome type 1F. Nat Commun 14, 2400. 10.1038/s41467-023-38038-y.

21. Johnson, K.R., Tian, C., Gagnon, L.H., Jiang, H., Ding, D., and Salvi, R. (2017). Effects of Cdh23 single nucleotide substitutions on age-related hearing loss in C57BL/6 and 129S1/Sv mice and comparisons with congenic strains. Sci Rep 7, 44450. 10.1038/srep44450.

22. Karali, M., Testa, F., Di Iorio, V., Torella, A., Zeuli, R., Scarpato, M., Romano, F., Onore, M.E., Pizzo, M., Melillo, P., Brunetti-Pierri, R., et al. (2022). Genetic epidemiology of inherited retinal diseases in a large patient cohort followed at a single center in Italy. Sci Rep 12, 20815. 10.1038/s41598-022-24636-1.

23. Koehler, K.R., Nie, J., Longworth-Mills, E., Liu, X.P., Lee, J., Holt, J.R., and Hashino, E. (2017). Generation of inner ear organoids containing functional hair cells from human pluripotent stem cells. Nat Biotechnol 35, 583-589. 10.1038/nbt.3840.

24. Lau, S.C., Grati, M., Isgrig, K., Sinan, M., Calabro, K.R., Zhu, J., Ishibashi, Y., Ozgur, Z., Wafa, T., Belyantseva, I.A., Fitzgerald, T., et al. (2023). Dual-AAV vector-mediated expression of MYO7A improves vestibular function in a mouse model of Usher syndrome 1B. Mol Ther Methods Clin Dev 30, 534-545. 10.1016/j.omtm.2023.08.012.

25. Lee, J., Nist-Lund, C., Solanes, P., Goldberg, H., Wu, J., Pan, B., Schneider, B.L., and Holt, J.R. (2020). Efficient viral transduction in mouse inner ear hair cells with utricle injection and AAV9-PHP.B. Hear Res 394, 107882. 10.1016/j.heares.2020.107882.

26. Lenassi, E., Saihan, Z., Bitner-Glindzicz, M., and Webster, A.R. (2014). The effect of the common c.2299delG mutation in USH2A on RNA splicing. Exp Eye Res 122, 9-12. 10.1016/j.exer.2014.02.018.

27. Lentz, J.J., Jodelka, F.M., Hinrich, A.J., McCaffrey, K.E., Farris, H.E., Spalitta, M.J., Bazan, N.G., Duelli, D.M., Rigo, F., and Hastings, M.L. (2013). Rescue of hearing and vestibular function by antisense oligonucleotides in a mouse model of human deafness. Nat Med 19, 345-350. 10.1038/nm.3106.

28. Lentz, J.J., Pan, B., Ponnath, A., Tran, C.M., Nist-Lund, C., Galvin, A., Goldberg, H., Robillard, K.N., Jodelka, F.M., Farris, H.E., Huang, J., et al. (2020). Direct Delivery of Antisense Oligonucleotides to the Middle and Inner Ear Improves Hearing and Balance in Usher Mice. Mol Ther 28, 2662-2676. 10.1016/j.ymthe.2020.08.002.

29. Lesman, D., Rodriguez, Y., Rajakumar, D., and Wein, N. (2021). U7 snRNA, a Small RNA with a Big Impact in Gene Therapy. Hum Gene Ther 32, 1317-1329. 10.1089/hum.2021.047.

30. Li, W., Jiang, X.S., Han, D.M., Gao, J.Y., Yang, Z.T., Jiang, L., Zhang, Q., Zhang, S.H., Gao, Y., Wu, J.H., and Li, J.K. (2022). Genetic Characteristics and Variation Spectrum of USH2A-Related Retinitis Pigmentosa and Usher Syndrome. Front Genet 13, 900548. 10.3389/fgene.2022.900548.

31. Liu, X., Bulgakov, O.V., Darrow, K.N., Pawlyk, B., Adamian, M., Liberman, M.C., and Li, T. (2007). Usherin is required for maintenance of retinal photoreceptors and normal development of cochlear hair cells. Proc Natl Acad Sci U S A 104, 4413-4418. 10.1073/pnas.0610950104.

32. Meunier, A., Zanlonghi, X., Roux, A.F., Fils, J.F., Caspers, L., Migeotte, I., Abramowicz, M., and Meunier, I. (2022). Natural history of Usher type 2 with the c.2299delG mutation of USH2A in a large cohort. Ophthalmic Genet 43, 470-475. 10.1080/13816810.2022.2051191.

33. Meyer, J.S., Howden, S.E., Wallace, K.A., Verhoeven, A.D., Wright, L.S., Capowski, E.E., Pinilla, I., Martin, J.M., Tian, S., Stewart, R., Pattnaik, B., et al. (2011). Optic vesicle-like structures derived from human pluripotent stem cells facilitate a customized approach to retinal disease treatment. Stem Cells 29, 1206-1218. 10.1002/stem.674.

34. Moraru, A.D., Costin, D., Iorga, R.E., Munteanu, M., Moraru, R.L., and Branisteanu, D.C. (2022). Current trends in gene therapy for retinal diseases (Review). Exp Ther Med 23, 26. 10.3892/etm.2021.10948.

35. Muller, A., Sullivan, J., Schwarzer, W., Wang, M., Park-Windhol, C., Hasler, P.W., Janeschitz-Kriegl, L., Duman, M., Klingler, B., Matsell, J., Hostettler, S.M., et al. (2025). High-efficiency base editing in the retina in primates and human tissues. Nat Med 31, 490-501. 10.1038/s41591-024-03422-8.

36. Nguyen, V.P., Song, J., Prieskorn, D., Zou, J., Li, Y., Dolan, D., Xu, J., Zhang, J., Jayasundera, K.T., Yang, J., Raphael, Y., et al. (2023). USH2A Gene Mutations in Rabbits Lead to Progressive Retinal Degeneration and Hearing Loss. Transl Vis Sci Technol 12, 26. 10.1167/tvst.12.2.26.

37. Pan, B., Askew, C., Galvin, A., Heman-Ackah, S., Asai, Y., Indzhykulian, A.A., Jodelka, F.M., Hastings, M.L., Lentz, J.J., Vandenberghe, L.H., Holt, J.R., et al. (2017). Gene therapy restores auditory and vestibular function in a mouse model of Usher syndrome type 1c. Nat Biotechnol 35, 264-272. 10.1038/nbt.3801.

38. Panagiotopoulos, A.L., Karguth, N., Pavlou, M., Bohm, S., Gasparoni, G., Walter, J., Graf, A., Blum, H., Biel, M., Riedmayr, L.M., and Becirovic, E. (2020). Antisense Oligonucleotide- and CRISPR-Cas9-Mediated Rescue of mRNA Splicing for a Deep Intronic CLRN1 Mutation. Mol Ther Nucleic Acids 21, 1050-1061. 10.1016/j.omtn.2020.07.036.

39. Pendse, N.D., Lamas, V., Pawlyk, B.S., Maeder, M.L., Chen, Z.Y., Pierce, E.A., and Liu, Q. (2019). In Vivo Assessment of Potential Therapeutic Approaches for USH2A-Associated Diseases. Adv Exp Med Biol 1185, 91-96. 10.1007/978-3-030-27378-1_15.

40. Qi, J., Tan, F., Zhang, L., Lu, L., Zhang, S., Zhai, Y., Lu, Y., Qian, X., Dong, W., Zhou, Y., Zhang, Z., et al. (2024). AAV-Mediated Gene Therapy Restores Hearing in Patients with DFNB9 Deafness. Adv Sci (Weinh) 11, e2306788. 10.1002/advs.202306788.

41. Riaz, S., Sethna, S., Duncan, T., Naeem, M.A., Redmond, T.M., Riazuddin, S., Riazuddin, S., Carvalho, L.S., and Ahmed, Z.M. (2023). Dual AAV-based PCDH15 gene therapy achieves sustained rescue of visual function in a mouse model of Usher syndrome 1F. Mol Ther 31, 3490-3501. 10.1016/j.ymthe.2023.10.017.

42. Roberts, C.L., Chen, S.S., Murchison, A.C., Ogle, R.A., Francis, M.P., Ogle, R.C., and Sachs, P.C. (2017). Preferential Lineage-Specific Differentiation of Osteoblast-Derived Induced Pluripotent Stem Cells into Osteoprogenitors. Stem Cells Int 2017, 1513281. 10.1155/2017/1513281.

43. Ross, M., Obolensky, A., Averbukh, E., Desrosiers, M., Ezra-Elia, R., Honig, H., Yamin, E., Rosov, A., Dvir, H., Gootwine, E., Banin, E., et al. (2022). Outer retinal transduction by AAV2-7m8 following intravitreal injection in a sheep model of CNGA3 achromatopsia. Gene Ther 29, 624-635. 10.1038/s41434-021-00306-1.

44. Sanjurjo-Soriano, C., Jimenez-Medina, C., Erkilic, N., Cappellino, L., Lefevre, A., Nagel-Wolfrum, K., Wolfrum, U., Van Wijk, E., Roux, A.F., Meunier, I., and Kalatzis, V. (2023). USH2A variants causing retinitis pigmentosa or Usher syndrome provoke differential retinal phenotypes in disease-specific organoids. HGG Adv 4, 100229. 10.1016/j.xhgg.2023.100229.

45. Shubina-Oleinik, O., Nist-Lund, C., French, C., Rockowitz, S., Shearer, A.E., and Holt, J.R. (2021). Dual-vector gene therapy restores cochlear amplification and auditory sensitivity in a mouse model of DFNB16 hearing loss. Sci Adv 7, eabi7629. 10.1126/sciadv.abi7629.

46. Slijkerman, R.W., Vache, C., Dona, M., Garcia-Garcia, G., Claustres, M., Hetterschijt, L., Peters, T.A., Hartel, B.P., Pennings, R.J., Millan, J.M., Aller, E., et al. (2016). Antisense Oligonucleotide-based Splice Correction for USH2A-associated Retinal Degeneration Caused by a Frequent Deep-intronic Mutation. Mol Ther Nucleic Acids 5, e381. 10.1038/mtna.2016.89.

47. Steinhart, M.R., van der Valk, W.H., Osorio, D., Serdy, S.A., Zhang, J., Nist-Lund, C., Kim, J., Moncada-Reid, C., Sun, L., Lee, J., and Koehler, K.R. (2023). Mapping oto-pharyngeal development in a human inner ear organoid model. Development 150. 10.1242/dev.201871.

48. Steinhart, M.R., van der Valk, W.H., Osorio, D., Serdy, S.A., Zhang, J., Nist-Lund, C., Kim, J., Moncada-Reid, C., Sun, L., Lee, J., and Koehler, K.R. (2023). Mapping oto-pharyngeal development in a human inner ear organoid model. Development 150. 10.1242/dev.201871.

49. Suarez-Herrera, N., Riswick, I.B., Vazquez-Dominguez, I., Duijkers, L., Karjosukarso, D.W., Piccolo, D., Bauwens, M., De Baere, E., Cheetham, M.E., Garanto, A., and Collin, R.W.J. (2024). Proof-of-concept for multiple AON delivery by a single U7snRNA vector to restore splicing defects in ABCA4. Mol Ther 32, 837-851. 10.1016/j.ymthe.2024.01.019.

50. Tebbe, L., Mwoyosvi, M.L., Crane, R., Makia, M.S., Kakakhel, M., Cosgrove, D., Al-Ubaidi, M.R., and Naash, M.I. (2023). The usherin mutation c.2299delG leads to its mislocalization and disrupts interactions with whirlin and VLGR1. Nat Commun 14, 972. 10.1038/s41467-023-36431-1.

51. van der Valk, W.H., van Beelen, E.S.A., Steinhart, M.R., Nist-Lund, C., Osorio, D., de Groot, J., Sun, L., van Benthem, P.P.G., Koehler, K.R., and Locher, H. (2023). A single-cell level comparison of human inner ear organoids with the human cochlea and vestibular organs. Cell Rep 42, 112623. 10.1016/j.celrep.2023.112623.

52. Velde, H.M., Reurink, J., Held, S., Li, C.H.Z., Yzer, S., Oostrik, J., Weeda, J., Haer-Wigman, L., Yntema, H.G., Roosing, S., Pauleikhoff, L., et al. (2022). Usher syndrome type IV: clinically and molecularly confirmed by novel ARSG variants. Hum Genet 141, 1723-1738. 10.1007/s00439-022-02441-0.

53. Wang, H., Xun, M., Tang, H., Zhao, J., Hu, S., Zhang, L., Lv, J., Wang, D., Chen, Y., Liu, J., Li, G.L., et al. (2024). Hair cell-specific Myo15 promoter-mediated gene therapy rescues hearing in DFNB9 mouse model. Mol Ther Nucleic Acids 35, 102135. 10.1016/j.omtn.2024.102135.

54. Wu, J., Solanes, P., Nist-Lund, C., Spataro, S., Shubina-Oleinik, O., Marcovich, I., Goldberg, H., Schneider, B.L., and Holt, J.R. (2021). Single and Dual Vector Gene Therapy with AAV9-PHP.B Rescues Hearing in Tmc1 Mutant Mice. Mol Ther 29, 973-988. 10.1016/j.ymthe.2020.11.016.

55. Yan, D., Ouyang, X., Patterson, D.M., Du, L.L., Jacobson, S.G., and Liu, X.Z. (2009). Mutation analysis in the long isoform of USH2A in American patients with Usher Syndrome type II. J Hum Genet 54, 732-738. 10.1038/jhg.2009.107.

56. Zhong, X., Gutierrez, C., Xue, T., Hampton, C., Vergara, M.N., Cao, L.H., Peters, A., Park, T.S., Zambidis, E.T., Meyer, J.S., Gamm, D.M., et al. (2014). Generation of three-dimensional retinal tissue with functional photoreceptors from human iPSCs. Nat Commun 5, 4047. 10.1038/ncomms5047.

57. Zou, J., Mathur, P.D., Zheng, T., Wang, Y., Almishaal, A., Park, A.H., and Yang, J. (2015). Individual USH2 proteins make distinct contributions to the ankle link complex during development of the mouse cochlear stereociliary bundle. Hum Mol Genet 24, 6944-6957. 10.1093/hmg/ddv398.

FIGURE CAPTIONS

Figure 1: **Generation and characterization of *Ush2a*$^{KO-1}$ mice** . (**A)** Schematic of the *Ush2a*$^{KO-1}$ mice model; (**B-D**) Click ABR recordings on WT (black) and *Ush2a*$^{KO-1}$ (magenta) mice at 4 weeks old (mean ± S.D. control: 46.43 ± 5.56 dB SPL (*n* = 7) and *Ush2a*$^{KO-1}$: 44.50 ± 3.69 dB SPL (*n* = 10), ns p = 0.5193, Mann–Whitney test) (**B**), 16 weeks old (mean ± S.D. control: 45.00 ± 6.33 dB SPL (*n* = 6); *Ush2a*$^{KO-1}$: 46.82 ± 3.37 dB SPL (*n* = 11) ns p = 0.7353, Mann–Whitney test) (**C**); 42 weeks old (mean ± S.D. control: 40.00 ± 0.00 dB SPL (*n* = 3); *Ush2a*$^{KO-1}$: 40.00 ± 5.00 dB SPL (*n* = 3), ns p > 0.9999, Mann–Whitney test) (**D**); (**E-G**) Pure-tone ABR recordings as a function of frequencies (kHz) on WT (black) and *Ush2a*$^{KO-1}$ (magenta) mice at 4 weeks (mean ± S.D. 5.6 kHz: ns p > 0.9999, 8.0 kHz: ns p = 0.6130, 11.3 kHz: ns p = 0.6736, 16.0 kHz: ns p > 0.9999, 22.6 kHz: ns p = 0.0801, 32.0 kHz: ns p = 0.7804; 2-way ANOVA Bonferroni's multi-comparison test) (**E**), 16 weeks old (mean ± S.D. 5.6 kHz: ns p > 0.9999, 8.0 kHz: ns p > 0.9999, 11.3 kHz: ns p > 0.9999, 16.0 kHz: ns p > 0.9999, 22.6 kHz: ns p > 0.9999, 32.0 kHz: ns p > 0.9999, 2-way ANOVA Bonferroni's multi-comparison test) (**F**), 42 weeks old (mean ± S.D. 5.6 kHz: ns p > 0.9999, 8.0 kHz: ns p = 0.8695, 11.3 kHz: ns p > 0.9999, 16.0 kHz: ns p > 0.9999, 22.6 kHz: ns p = 0.1465, 32.0 kHz: ns p = 0.1465, 2-way ANOVA Bonferroni's multi-comparison test) (**G**); (**H-J**) Distortion-product otoacoustic emissions (DPOAEs) recordings as a function of frequencies (kHz) on WT (black) and *Ush2a*$^{KO-1}$ (magenta) mice at 4 weeks old (mean ± S.D. 5.6 kHz: ns p > 0.9999, 8.0 kHz: ns p > 0.9999, 11.3 kHz: ns p = 0.6787, 16.0 kHz: ns p > 0.9999, 22.6 kHz: ns p > 0.9999, 32.0 kHz: ns p > 0.9999, 45.2 kHz: *** p = 0.0005, 2-way ANOVA Bonferroni's multi-comparison test) (**H**), 16 weeks old (mean ± S.D. 5.6 kHz: ns p > 0.9999, 8.0 kHz: ns p > 0.9999, 11.3 kHz: ns p > 0.9999, 16.0 kHz: ns p > 0.9999, 22.6 kHz: ns p > 0.9999, 32.0 kHz: ns p > 0.9999, 45.2 kHz: * p = 0.0160; 2-way ANOVA Bonferroni's multi-comparison test) **(I),** and 42 weeks old (mean ± S.D. 5.6 kHz: ns p > 0.9999, 8.0 kHz: ns p > 0.9999, 11.3 kHz: ns p > 0.9999, 16.0 kHz: ns p > 0.9999, 22.6 kHz: ns p > 0.9999, 32.0 kHz: ns p > 0.9999, 45.2 kHz: ns p = 0.0502, 2-way ANOVA Bonferroni's multi-comparison test) **(J - K)** Average of individual click ABR wave 1 traces of highest intensity tested (90, 80, and 70 dB SPL) in WT (black) and *Ush2a*$^{KO-1}$ (magenta) mice at 4 and 16 weeks old. The black arrowhead indicates the positive peak of wave 1 (P1), and the red arrowhead indicates the negative peak of wave 1 (N1); **(L)** Measurement of wave 1 amplitude (N1-P1) at the highest intensities tested (90, 80, and 70 dB

SPL) during click recordings in WT (black) and *Ush2a*$^{KO-1}$ (magenta) mice at 4 and 16 weeks old (mean ± S.D. 4 weeks old: control: 2.77 ± 0.77 µV (*n* = 7); *Ush2a*$^{KO-1:}$ 3.17 ± 0.84 µV (*n* = 11); ns p = 0.3283, Mann–Whitney test, and 16 weeks old control: 1.68 ± 0.39 µV (*n* = 6); *Ush2a*$^{KO-1}$: 2.06 ± 0.84 µV (*n* = 6); ns p = 0.6667, Mann–Whitney test); (**M**) Measurement of wave 1 latency (N1-P1) at the highest intensities tested (90, 80, and 70 dB SPL) during click recordings in WT (black) and *Ush2a*$^{KO-1}$ (magenta) mice at 4 and 16 weeks old (mean ± S.D. 4 weeks old: control: 1.40 ± 0.27 ms (*n* = 7); *Ush2a*$^{KO-1}$: 1.27 ± 0.09 ms (*n* = 11); ns p = 0.6430, Mann–Whitney test; 16 weeks old : control: 1.19 ± 0.05 ms (*n* = 6); *Ush2a*$^{KO-1}$: 1.26 ± 0.07 ms (*n* = 6); ns p = 0.1299, Mann–Whitney test).

Figure 2: **Morphological and Molecular Characterization of *Ush2a*$^{KO-1}$ mice. (A)** Confocal images of the organ of Corti at the apex, mid, and base in control mice (*Ush2a*$^{+/KO-1}$) and *Ush2a*$^{KO-1}$ mice at 16 weeks old. Phalloidin (grey). Orange squares highlight zoomed-in views of OHC bundles (upper right panels) and IHCs bundles (lower right panels). Scale bars: 5 µm (overview) and 1 µm (zoomed-in); **(B-C)** RT-PCR performed on inner ears **(B)** or eyes **(C)** harvested from WT and *Ush2a*$^{KO-1}$ mice between post-natal stages 5 (P) and P6. Red dotted boxes indicate exon 12 skipping. Size bands: control: full-length = 1301 bp, Exon 12 skip = 659 bp, partial Exon 12 skip = 869 bp; *Ush2a*$^{KO-1}$: full-length = 1205 bp, Exon 12 skip = 659 bp, partial Exon 12 skip = 869 bp.

Figure 3: Endogenous *USH2A* exon 13 skipping in inner ear organoid (IEOs) and retinal organoid (ROs) (A) Schematic overview of inner ear and retinal organoid generation. The initial activation of BMP4 signaling determines the developmental trajectory, directing cells toward a non-neural ectoderm fate for inner ear differentiation or a neural ectoderm fate for retinal differentiation. IEOs achieve basic structural maturity around D35 of differentiation and beyond, and ROs reach this stage around D120 and beyond. Representative live-cell images of a D100 IEO and a D135 RO derived from SOX2-GFP hiPSCs show SOX2^{+} IEOs embedded within a large aggregate and the retinal neuroepithelium in the ROs. Scale bars, 300 µm; **(B)** RT-PCR performed on human control (IEO^{SOX2}) and *c.2299delG USH2A* IEOs (IEO^{C20}) at different stages, from D106 to D141; **(C)** RT-PCR performed on human control (RO^{SOX2}) and *c.2299delG USH2A* (RO^{C20}) ROs at different stages, from D128

to D183. Red dotted boxes indicate exon 13 skipping, and yellow dotted-boxes indicate dual skipping of exons 12 & 13. Size bands: full-length = 1301 bp, Exon 13 skip = 902 bp, Exon 12 & 13 skip = 706 bp.

Figure 4: Screening of human *USH2A* exon 13 U7 snRNA skippers. (A) eGFP reporter construct containing human *USH2A* exon 12 - intron 12 - exon 13 (*c.2299delG*) - intron 13 - exon 14 - eGFP. The construct was designed to express eGFP only when *USH2A* exon 13 skipping occured; **(B)** Quantification of skipper efficiency for 619 U7 snRNA skippers. eGFP signal values for U7 snRNA skipper antisense sequences were normalized to the GFP signal of the QR-421a antisense sequence and are plotted as fold increase vs skipper number; **(C)** Representative example of a 96-well plate from which eGFP signal quantified in panel **B** was measured with ImageXpress Micro Confocal high content imager. Upper left: QR-AS (positive control, green box): U7 snRNA skipper construct encoding QR-421a antisense sequence; Non-specific skipper (negative control, red box): U7 snRNA skipper construct encoding non-hybridizing sequence. Mock (white box) corresponds to untreated condition; (**D)** Quantification eGFP intensity for single antisense snRNA skippers and dual antisense snRNA skippers.

Figure 5: Capsid screening in WT mice. (A) Schematic of the utricle injection procedure for virus delivery. At postnatal days (P) 1-2, 1 µL of each virus was injected through the utricle. Twenty AAV capsids were tested, each containing CMV promoter and encoding GFP; **(B)** Percentage of IHCs expressing eGFP. The values represent the infection efficiency of each capsid, assessed by the percentage of GFP-expressing cells, in the apex (A), mid (M), and base (B) of the cochleas of WT mice; **(C)** Same quantification as in panel B but for OHCs. Red boxes highlight the most efficient capsids, i.e. AAV9-PHP.B (1), Bpo.394 (17) and AAV9-PHP.eB (20); Capsid numbers and corresponding names are listed in Figure S6.

Figure 6: Representative images of mouse cochleas and vestibular organs exposed to AAV vectors. Three different regions of the cochlea (apex, mid, and base) and the vestibular organs (utricle, saccule, and ampullas) imaged 10 days after virus injection. The cyan signal indicates GFP expression resulting from the viral

injection. The top rows of each capsid group (number 1, 20, and 17 from the Figure S5) show inner ear tissue at low magnification (x10), and the middle and bottom rows display the inner ear tissues at high magnification (x63).

Figure 7: **AAV9-PHP.B and AAV2-7m8 induce exon skipping in IEOs. (A)** Representative brightfield images showing early differentiation stages during control (IEO^{SOX2}) and mutant *c.2299delG USH2A* (IEO^{C20}) IEO generation. Aggregates develop multiple otic vesicles within a single large structure, as highlighted with SOX2 expression in representative immunostaining images on D35 of differentiation. Scale bars: 100 µm (D0 and D35 IEOs) and 250 µm; **(B)** Representative immunostaining images of IEOs on D35 of differentiation, confirming the development of $ECAD^+$ $SOX2^+$ otic epithelium. This epithelium comprises $PCP4^+$ $POU4F3^+$ sensory hair cells and $SOX2^+$ supporting cells, with $TUJ1^+$ neurons innervating the sensory epithelium and hair cells. Scale bars, 50 µm (bottom panel) and 100 µm; **(C)** Representative confocal images of a D118 IEO at 15 days-post transductions with AAV9-PHP.B-skipper-mKate (red), shown at low (x4, left panel) and high (x20, right panels) magnification. Incorporation of SiR-Actin (magenta) visualizes hair bundles. The white dotted-box indicates the area magnified in the right panels. Scale bars, 10 µm (right panels) and 500 µm (left panel); **(D)** RT-PCR performed on D79-87 IEO^{SOX2} (control) organoids harvested after being untreated (no virus) or transduced with the AAV9-PHP.B-skipper-mKate. The region between exons 10 and 16 was amplified. The full-length band is 1544bp, the band excluding exon 13 is 902 bp, and the band excluding both exons 12 and 13 is 706 bp; **(E)** RT-PCR performed on D106, D118, and D141 IEO^{SOX2} and IEO^{C20} harvested after being untreated (no virus) or treated with either the AAV9-PHP.B-skipper-mKate or AAV9-PHP.B-mKate-empty viruses. The region between exons 10 and 16 was amplified. The full-length band is 1544 bp, the band excluding exon 13 is 902 bp, and the band excluding both exons 12 and 13 is 706 bp. Control D141 IEO^{C20} untreated gel reprinted from Fig. 3B to facilitate comparison; **(F)** Semi-quantitative measurement performed on RT-PCR agarose gels of IEOs treated with either AAV9-PHP.B-skipper-mKate, AAV9-PHP.B-mKate-empty viruses, or left untreated for 14-16 days in culture. The age of IEOs was between D106 and D141. Bar graphs depict percent change in band intensity (from panel **E**) for *USH2A* exon 13 skip relative to full-length *USH2A* (mean ± S.D.); **(G)** RT-PCR performed on D73 IEO^{SOX2} and IEO^{C20} harvested after being untreated (no virus) or treated with either the AAV2-7m8-skipper-mKate or AAV2-7m8-GFP-empty viruses. The region between exons 10 and 16 was amplified. The full-length band is

1544 bp, the band excluding exon 13 is 902 bp, and the band excluding both exons 12 and 13 is 706 bp; **(H)** Semi-quantitative measurement performed on RT-PCR agarose gels of IEOs treated with either AAV2-7m8-skipper-mKate, AAV2-7m8-GFP-empty viruses, or left untreated for 14-16 days in culture. The age of IEOs is comprised between D67-73. Bar graphs depict percent change in band intensity (from panel **G**) for *USH2A* exon 13 skip relative to full-length *USH2A* (mean ± S.D.); **(I)** Representative confocal images of D63 IEO^{SOX2} and IEO^{C20} organoids that were untreated (no virus) or transduced with either the AAV2-7m8-skipper-mKate or AAV2-7m8-GFP-empty viruses. Incorporation of SiR-Actin illuminates putative otic vesicle (pOtV). The white dotted-lines indicate the area of a pOtV. Scale bars, 100 µm.

Figure 8: **AAV9-PHP.B and AAV2-7m8 induce exon skipping in ROs. (A)** Representative brightfield images showing early differentiation stages of RO^{SOX2} (control) and RO^{C20} (*c.2299delG USH2A*) generation. Developing retinal neuroepithelium (RN) is observed starting around D25 of differentiation. Representative SOX2 live-cell images on D12 highlights the presence of retinal progenitor cells. Scale bars, 100 µm; **(B)** Representative immunostaining images of D60 RO^{SOX2} and RO^{C20} at early differentiation stages. $SOX2^+$ $PAX6^+$ developing RN regions contain $CHX10^+$ retinal progenitor cells, which are expected to further differentiate into bipolar cells at later stages (e.g., D120+). $TUJ1^+$ developing neuronal cells, including retinal ganglion cells, are also present. Scale bars, 100 µm; **(C)** Representative live-cell images of D196 RO^{SOX2} transduced with AAV9-PHP.B-mKate-empty. Transduction efficiency is relatively low with the AAV9-PHP.B capsid (red). See *Video S3* and *Figure S7* for additional supporting data. Scale bars, 100 µm; **(D)** RT-PCR performed on D128, D162, and D183 RO^{SOX2} and RO^{C20} harvested after being untreated (no virus) or transduced with either AAV-PHP.B-skipper-mKate or AAV-PHP.B-mKate-empty viruses for 14-16 days in culture. The region between exons 10 and 16 was amplified. The full-length band is 1544 bp, the band excluding exon 13 is 902 bp, and the band excluding exons 12 & 13 is 706 bp. Control untreated gels at D162 and D183 reprinted from Fig. 3C to facilitate comparison; **(E)** Semi-quantitative measurement performed on RT-PCR agarose gels of ROs transduced with either AAV9-PHP.B-skipper-mKate or AAV9-PHP.B-mKate-empty viruses or left untreated for 14-16 days in culture. The age of ROs was between D128-183. Bar graphs depict percent change in band intensity (from panel D) for *USH2A* exon 13 skip relative to full-length *USH2A* (mean ± S.D.); **(F)** RT-PCR performed on D105 RO^{SOX2} and RO^{C20} harvested

after being untreated (no virus) or treated with either AAV2-7m8-skipper-mKate or AAV2-7m8-GFP-empty viruses for 14-16 days in culture. The region between exons 10 and 16 was amplified. The full-length band is 1544 bp, the band excluding exon 13 is 902 bp, and the band excluding both exons 12 and 13 is 706 bp; **(G)** Semi-quantitative measurement performed on RT-PCR agarose gels of ROs transduced with either AAV2-7m8-skipper-mKate or AAV2-7m8-GFP-empty viruses or left untreated for 14-16 days in culture. The age of ROs is D105. Bar graphs depict percent change in band intensity (from panel F) for USH2A exon 13 skip relative to full-length USH2A (mean ± S.D.); **(H)** Representative confocal images of D112 RO^{SOX2} and RO^{C20} that were either untreated (no virus) or transduced with either the AAV2-7m8-skipper-mKate or AAV2-7m8-GFP-empty viruses. Scale bars, 200 μm. See *Figure S7* for additional data.

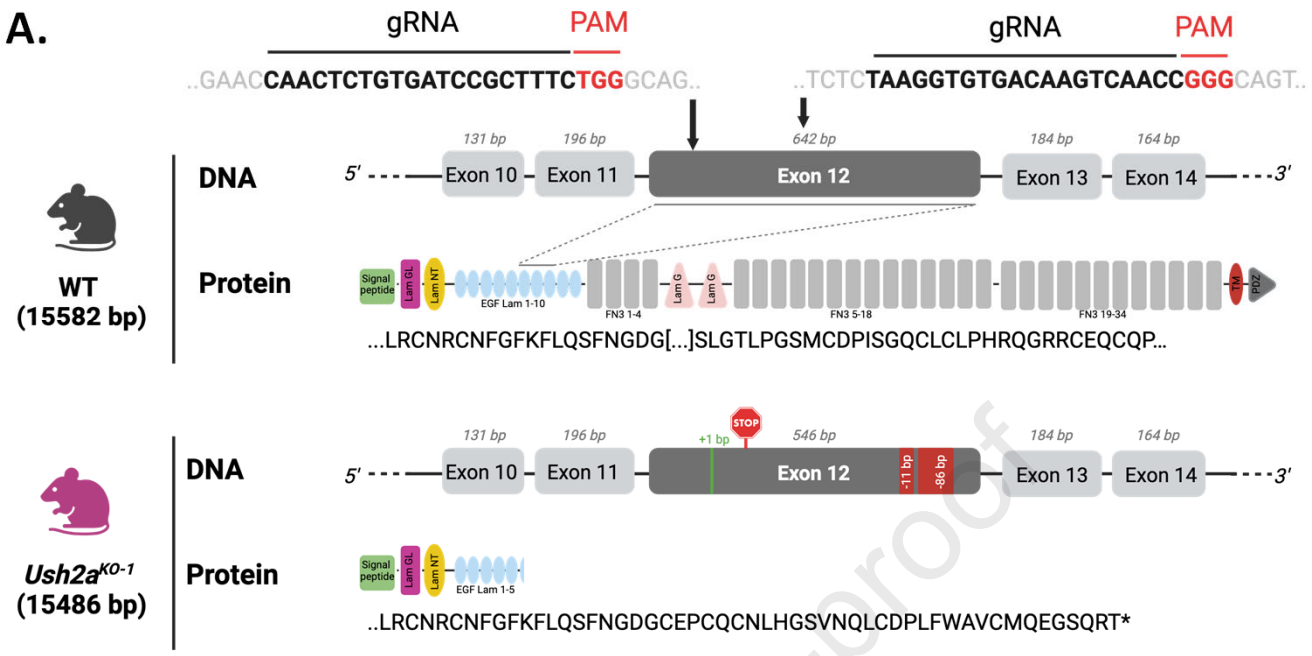

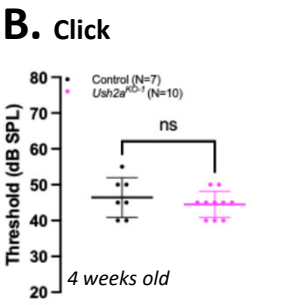

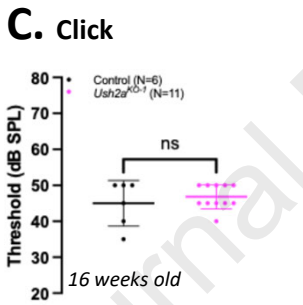

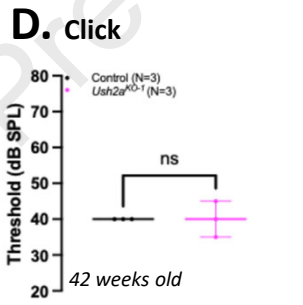

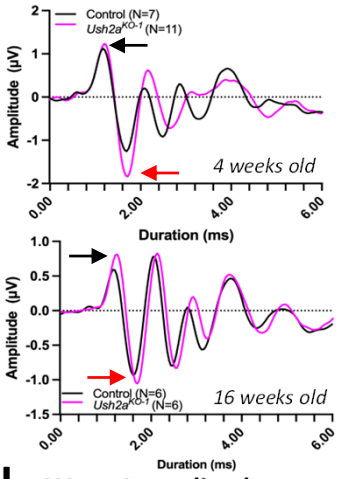

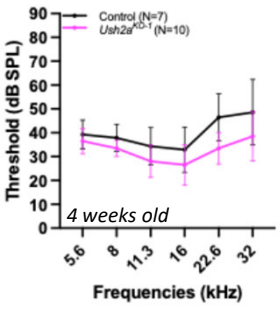

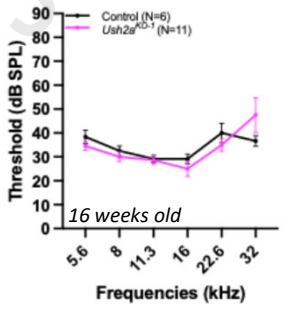

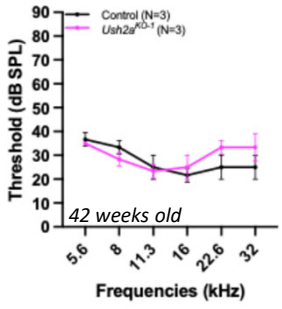

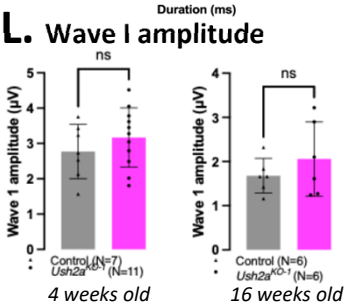

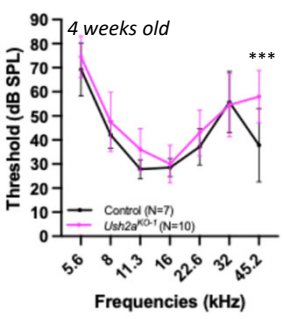

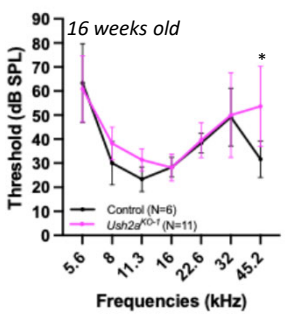

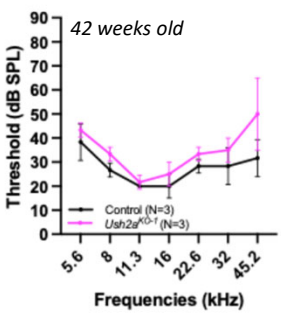

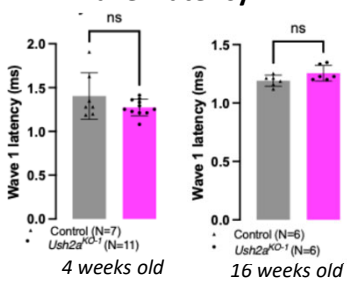

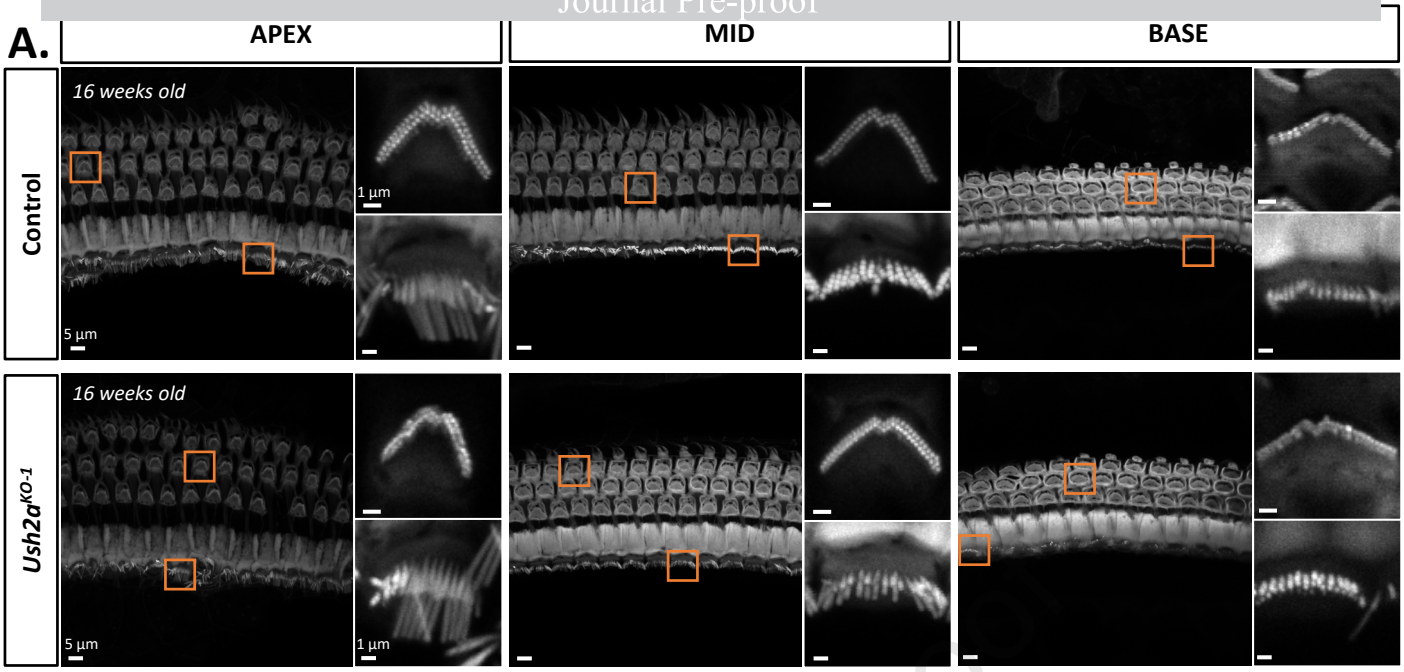

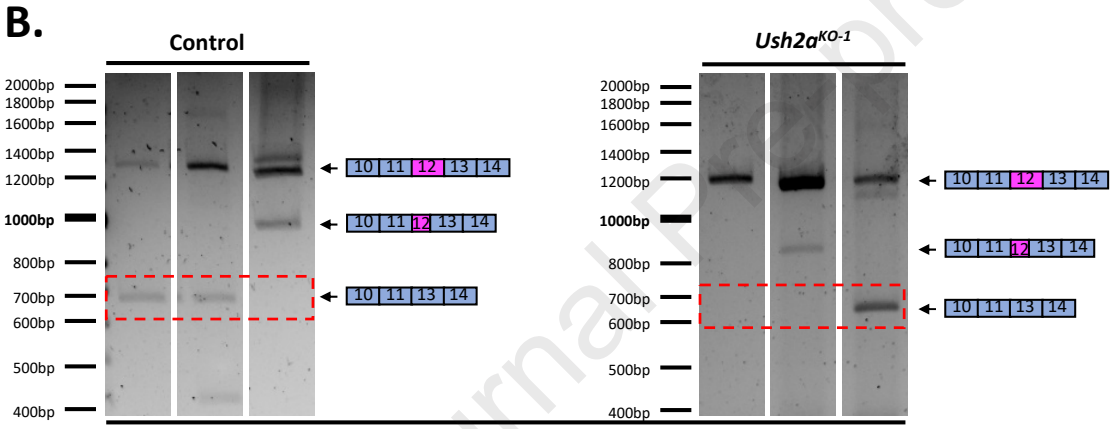

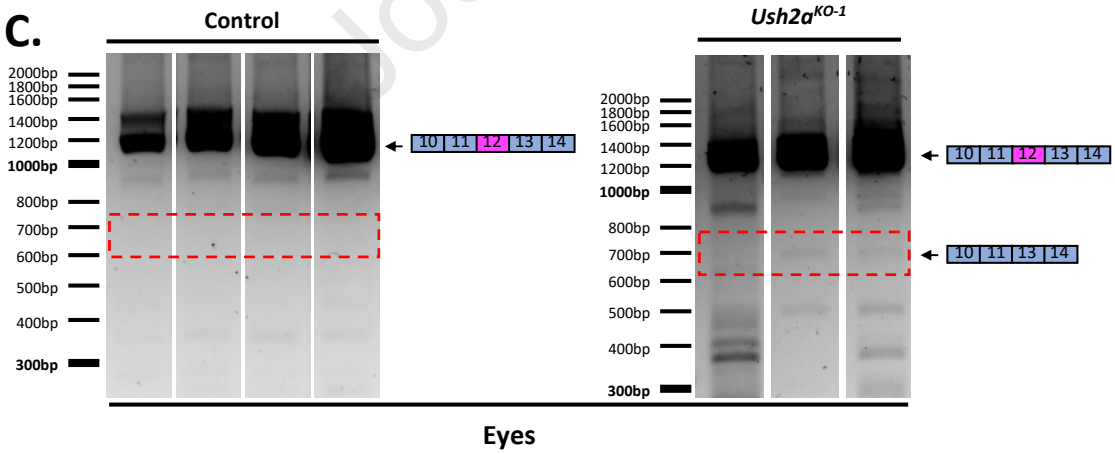

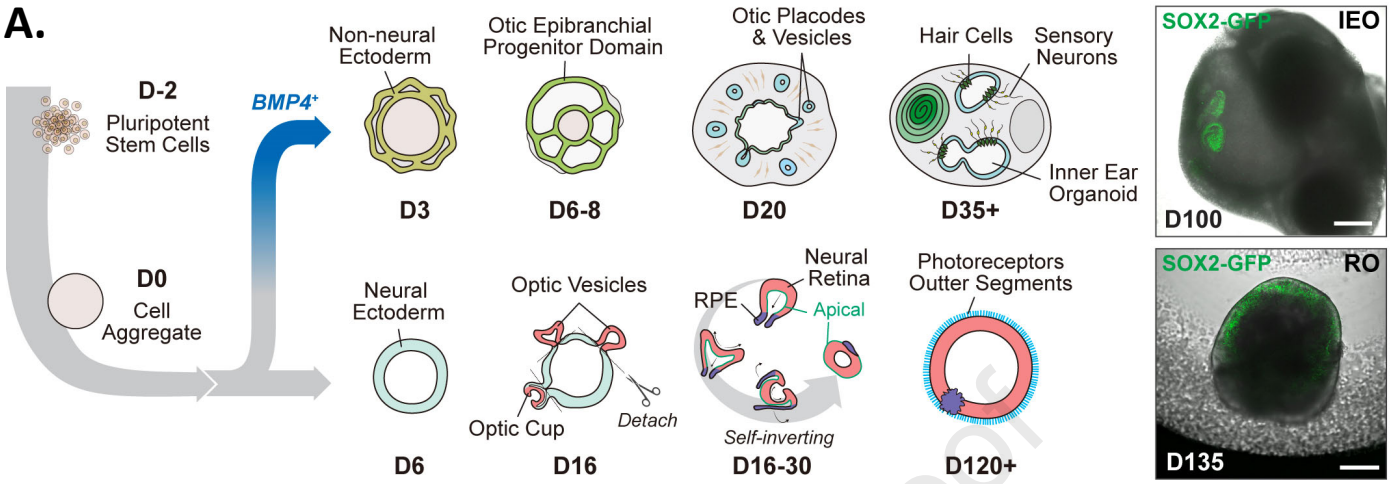

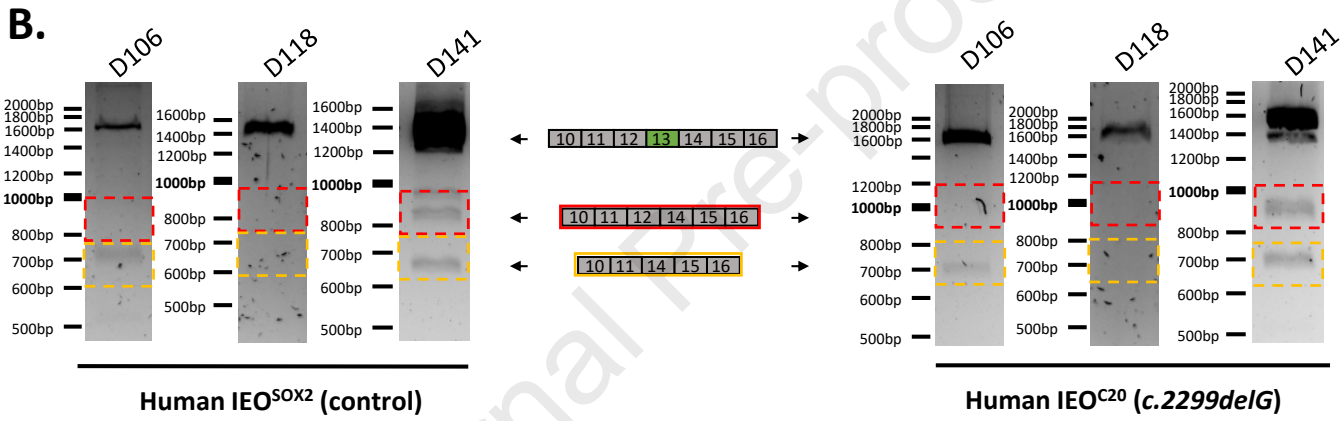

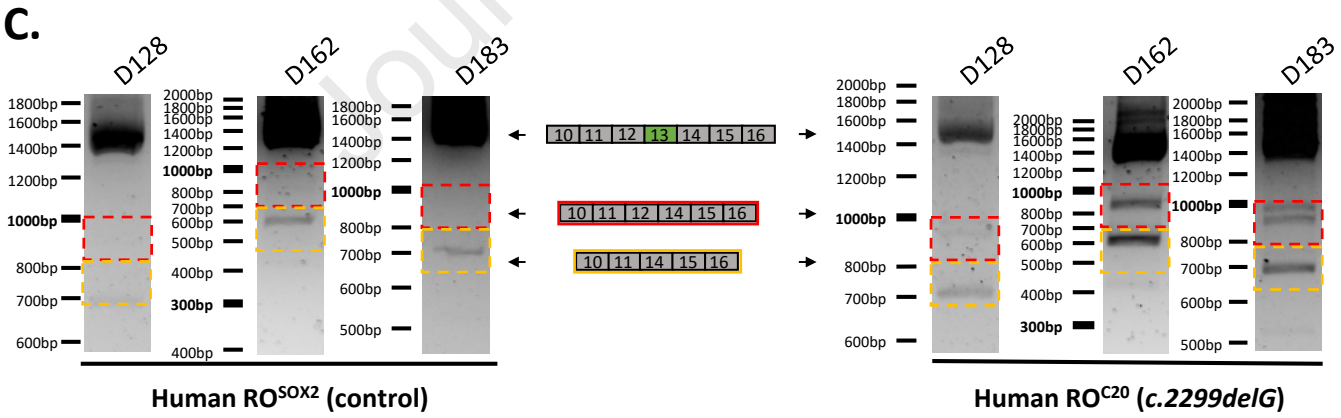


A.
c.2299delG
Stop codon
Reporter
Exon 12
Exon 13
Exon 14
EGFP
Stop codon
No skipping
Exon 13 skipping
No GFP expression
GFP expression =
successful Exon13 skipping

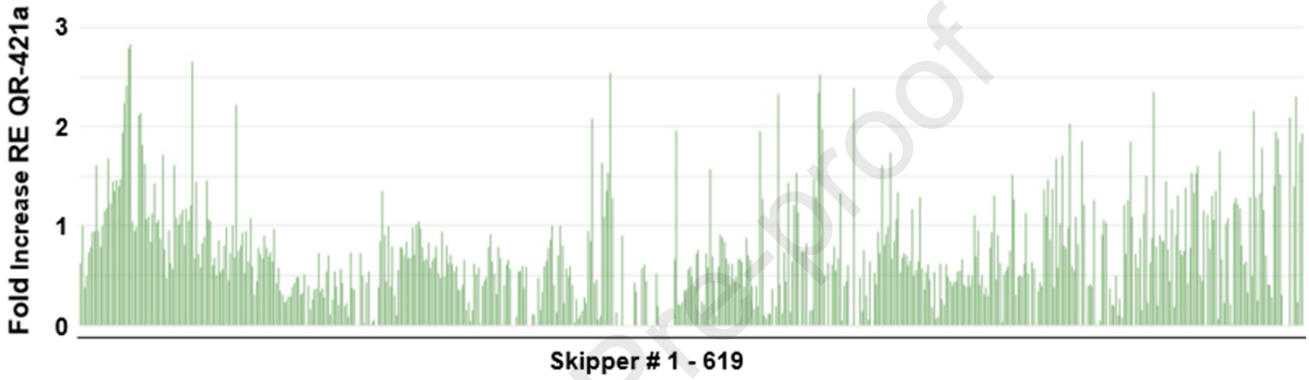
B.
Fold Increase RE QR-421a
3
2
1
0
Skipper # 1 - 619

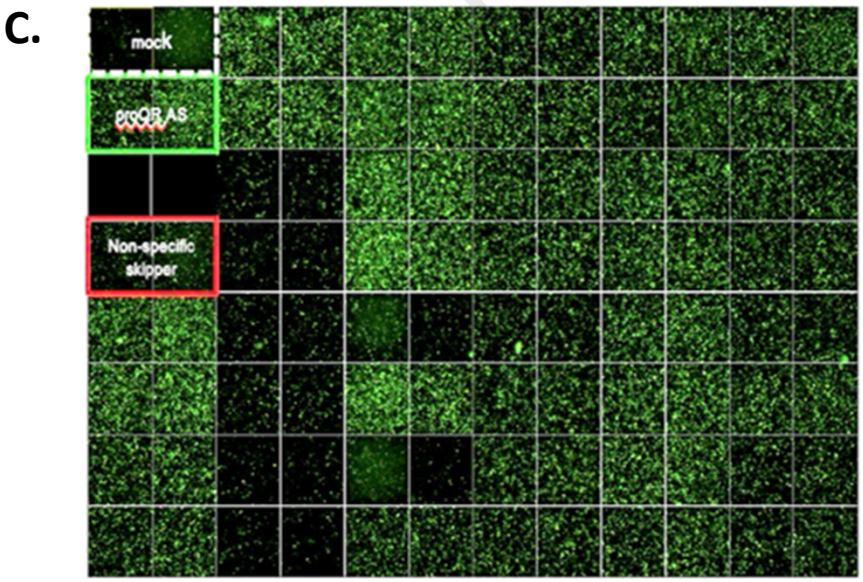
C.
mock
proQR AS
Non-specific
skipper

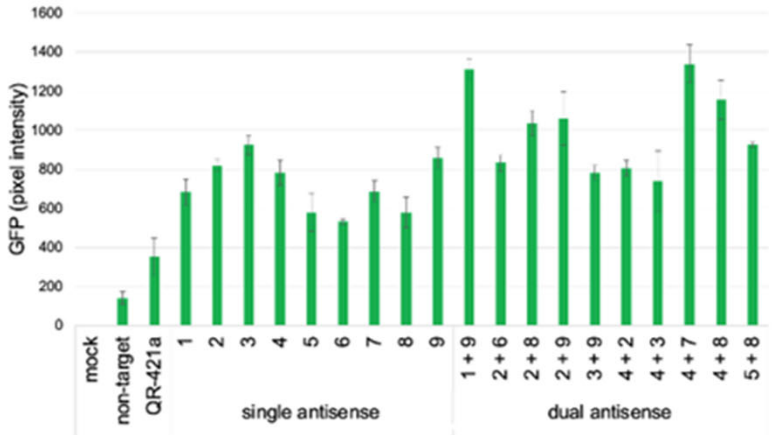
D.
GFP (pixel intensity)
1600
1400
1200
1000
800
600
400
200
0
mock
non-target
QR-421a
1
2
3
4
5
6
7
8
9
1 + 9
2 + 6
2 + 8
2 + 9
3 + 9
4 + 2
4 + 3
4 + 7
4 + 8
5 + 8
single antisense
dual antisense

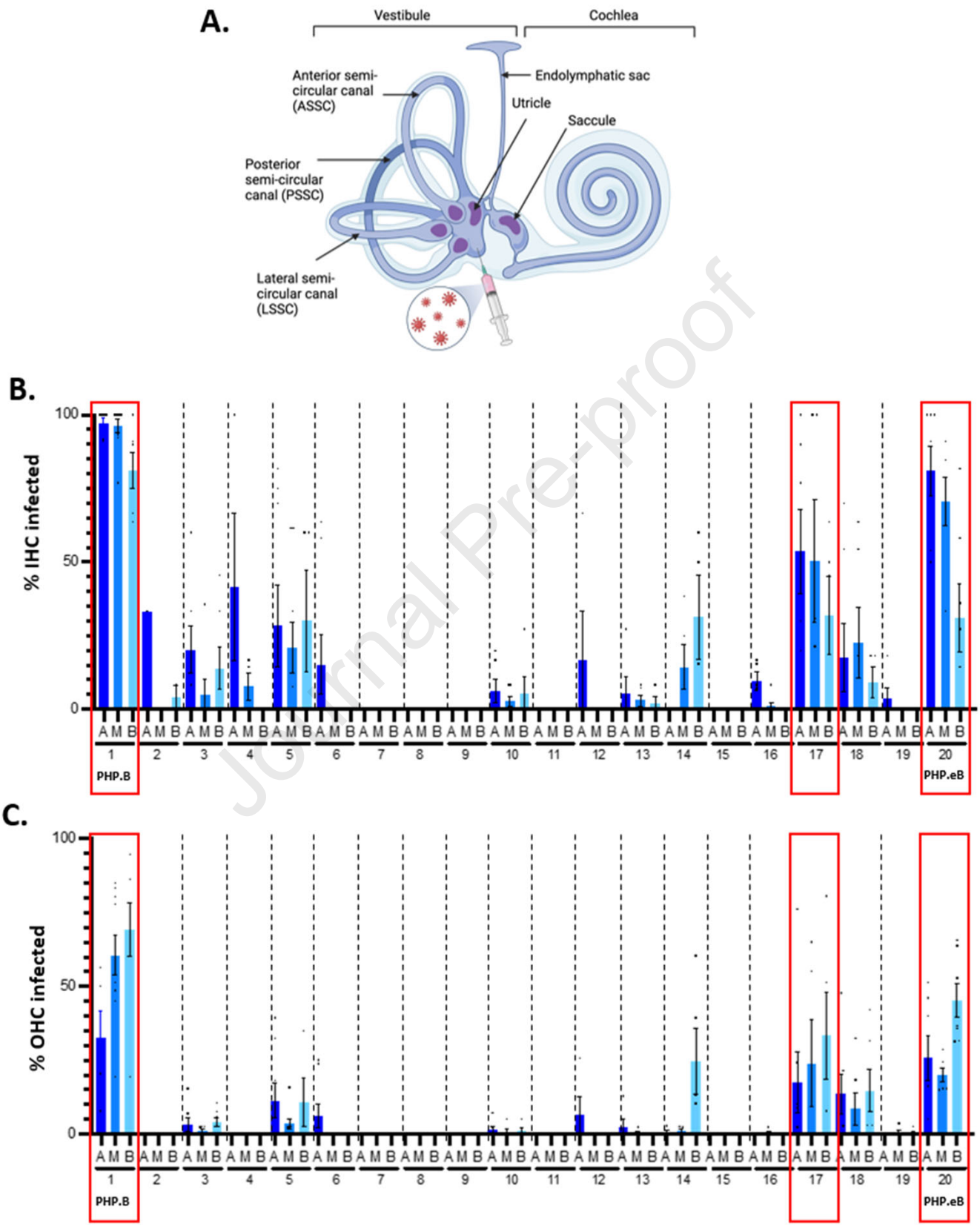

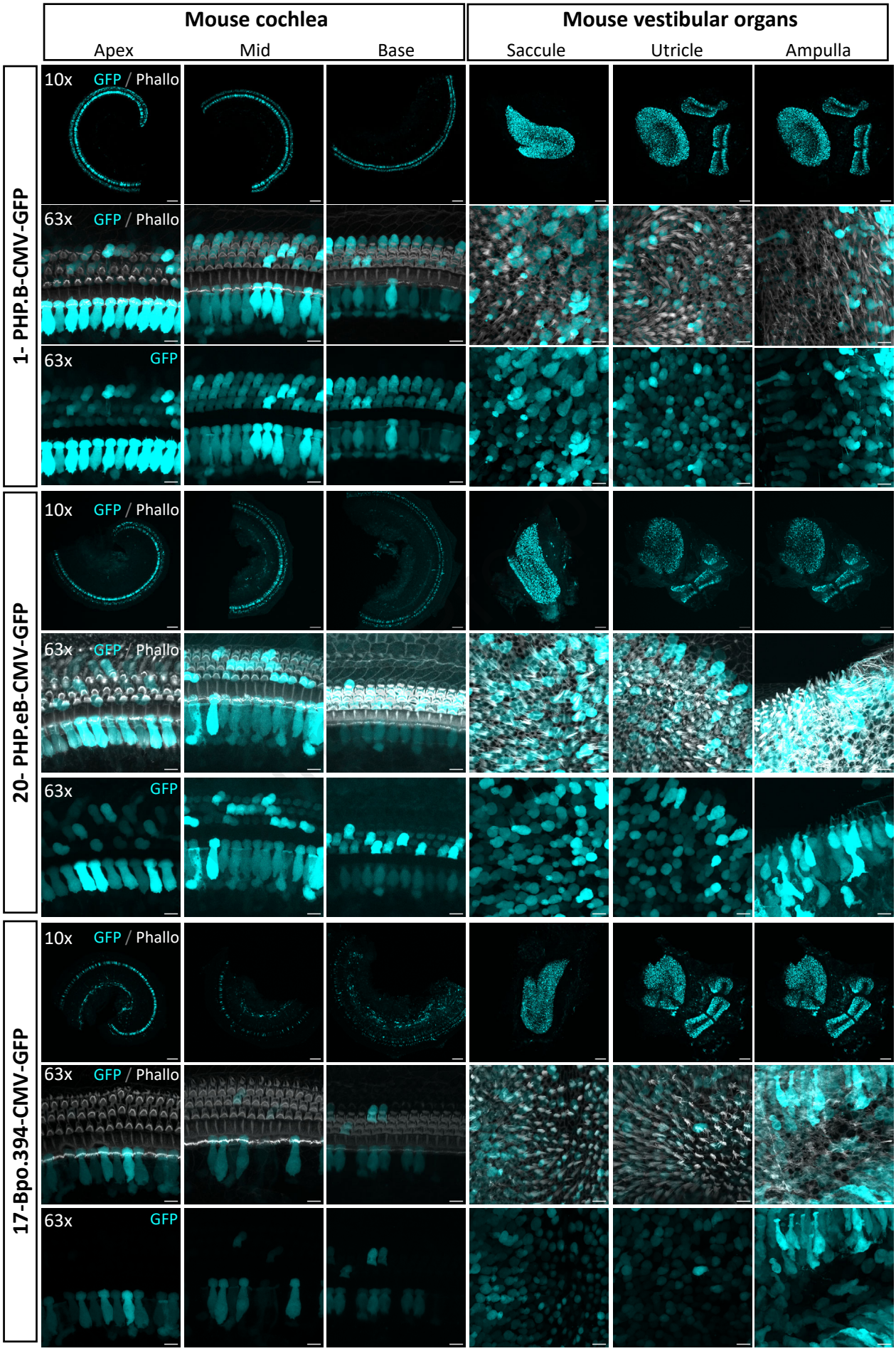
Mouse cochlea
Mouse vestibular organs
Apex
Mid
Base
Saccule
Utricle
Ampulla
1- PHP.B-CMV-GFP
20- PHP.eB-CMV-GFP
17-Bpo.394-CMV-GFP
10x GFP / Phallo
63x GFP / Phallo
63x GFP

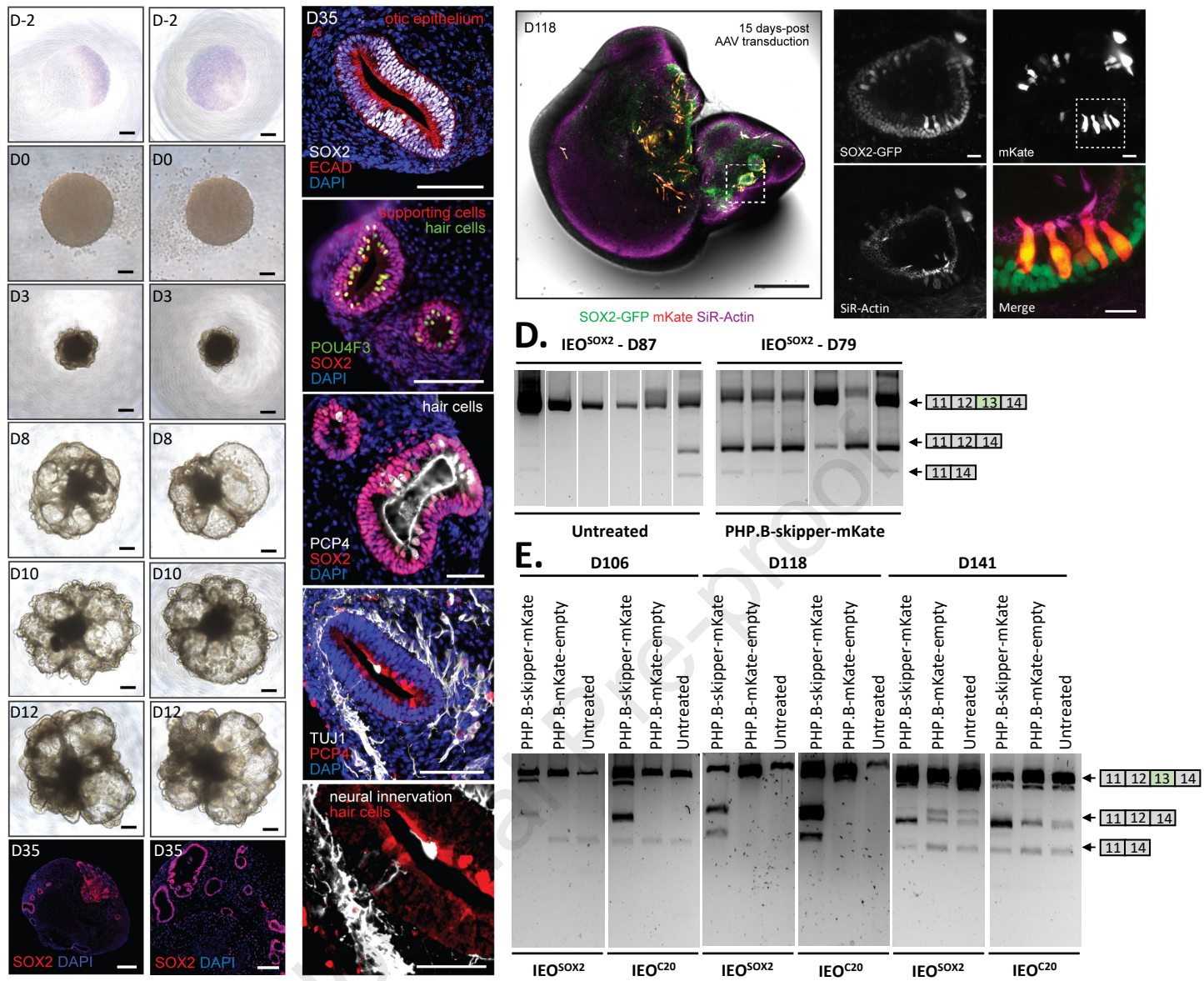

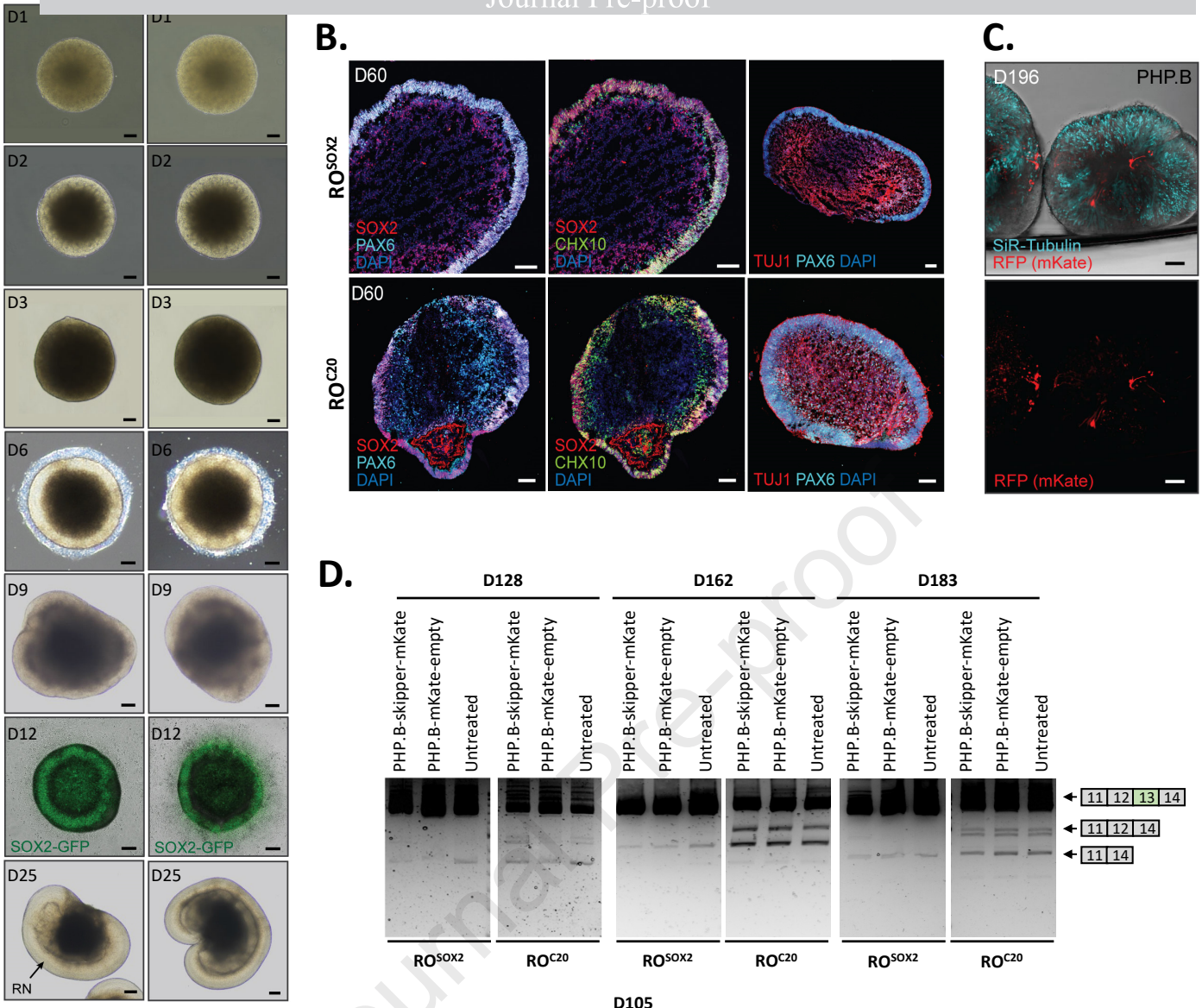

Géléoc and colleagues generated vectorized ASOs to enhance exon skipping. The ASOs were designed to bypass the most common Usher syndrome mutation, USH2A c.2299delG. Vectorized ASOs were tested in inner ear and retinal organoids harboring the c.2299delG mutation. Géléoc et al. report robust exon skipping in organoid hair cells and photoreceptors.